Thermodynamic Analysis of the Effect of Compression and Injection Quality Faults on DI Diesel Engine Combustion and Performance Characteristics

John S. Katsanis[a], Marios I. Kourampas[a], Elias A. Yfantis[a], Efthimios G. Pariotis[a] and Theodoros C. Zannis[a]

[a]*Naval Architecture and Marine Engineering Section, Hellenic Naval Academy, End of Hatzikiriakou Ave. 18539 Piraeus, Greece*

Abstract. In the present study a closed-cycle diesel engine simulation code based on a multi-zone combustion model was used to simulate three diesel engine faulty operation cases i.e. reduction of mean injection pressure, reduction of fuel injected mass per engine cycle and reduction of compression ratio. The multi-zone combustion model upon successful experimental validation was used to generate theoretical results for cylinder pressure, fuel evaporation rate and bulk gas temperature for each one of the previously mentioned engine faulty operation cases. The predicted cylinder pressure profiles were supplied to a computational model developed in MATLAB under a diploma thesis conducted in Hellenic Naval Academy in order to perform a heat release rate analysis and to derive the main performance characteristics of the examined diesel engine. The MATLAB model was used to derive results for heat release rate, heat losses rate, ignition angle and ignition delay and premixed phase, diffusion-controlled and total combustion durations. The assessment of all theoretical results for combustion parameters and engine performance characteristics showed that the reduction of mean injection pressure and the pertinent reduction of compression ratio affected negatively the diesel engine combustion mechanism by decreasing ignition angle and thus, shifting combustion event to the expansion stroke and, by increasing total combustion duration. The reduction of fuel consumption resulted in noticeable reduction of engine power and efficiency due to reduction of engine supplied heating power whereas, it did not affect seriously the time evolution of the combustion event inside the combustion chamber.

Keywords: diesel engine; injection pressure; fuel consumption; compression ratio; performance

INTRODUCTION

Diesel engine is world-known for its superior thermal efficiency among all other thermal engines [1]. The evolution of electronically-controlled fuel injection systems and the pertinent advances in turbocharging systems have led in the development of advanced technology diesel engines for various applications i.e. automotive, marine, electric power generation etc. with considerably lower brake specific fuel consumption (BSFC) and increased power density compared to recent past. As a characteristic example today marine four-stroke medium-speed

diesel engines have a minimum BSFC of 170 g/kWh whereas, the pertinent minimum BSFC of modern two-stroke slow-speed diesel engines is close to 156 g/kWh. Besides the need for minimization of specific fuel consumption and maximization of power density, there is a continuous requirement from diesel engines in all the fields of their application for high availability and reliability. The requirement for high availability from diesel engines is directly related with the minimization of the time that the engine is out of operation due to maintenance issues or in other words, is directly related with the unexpected faults of a diesel engine. Hence, it is of utmost importance not only the reduction of maintenance time by developing effective maintenance techniques but also the development of sophisticated techniques for the continuous monitoring and assessment of diesel engine operation and the utilization of monitoring data for the development of effective diagnostic techniques. Successful implementation of diagnostic techniques in diesel engines can lead to the tracking of a faulty operation cause by proposing specific measures for the healing of the specific problem and there are reported cases that diesel engine diagnosis have led to the prevention of catastrophic damages reducing thus, substantially the corresponding maintenance cost [2,3].

Studies performed in the past have demonstrated the multiple virtues of diesel engine monitoring and preventive maintenance technologies and have sorted the relative importance of various faulty situations often appeared in diesel engines [4,5]. Published studies have also exposed the beneficial effect of diesel engine continuous monitoring not only to the identification of faulty operation cases but also to diesel engine optimized operational and environmental behaviour [2,3,6]. Various technologies have been proposed in the literature for the monitoring and diagnosis mainly of large-type two-stroke slow-speed and heavy-duty four-stroke medium-speed marine diesel engines, which differ on the type of measuring data obtained from the engine and the pertinent technique used for their processing and assessment. One of the most prominent and world-known monitoring and diagnostic techniques is the one proposed by Hountalas et al. [2,3,7], which is based on the measurement of the cylinder pressure and the development of a sophisticated thermodynamic method for tracking TDC without measuring equipment and for processing the measured cylinder pressure data for assessing current diesel engine operational status, tracking the cause of unpleasant faulty situations and in such case proposing specific healing measures and for projecting its performance trends in the future. Another category of diesel engine diagnostic technique concerns the measurement of torsional vibrations and the processing the obtained torsional vibration data for tracking mainly the cylinder that does not contributing equally to the torsional vibration profile of the crankshaft [8,9]. The measurement and processing of torsional vibration data through that it can track faulty cylinder it cannot identify, unlike the previously mentioned thermodynamic method, the cause of faulty cylinder operation. Another technology proposed for diesel engine monitoring and diagnosis is the measurement and processing of mechanical vibration data obtained from various positions on the engine i.e. turbocharger, crankcase, camshaft case etc. [10,11]. The processing of vibration data is based on the derivation of RMS and the vibration spectrum for each diesel engine component and then the comparison of the derived vibration spectrum with exemplary vibration spectrums corresponding to specific faulty conditions such as shaft misalignment. Hence, though that the analysis of measured vibration data can identify the mechanical problem of a faulty engine component it cannot directly identify the potential thermo-fluid cause of this mechanical problem. Also, after-engine technologies such as diesel engine oil analysis have been extensively used for characterizing engine operational status [12]. The advancement of information

technology during recent years have also led to the implementation of information fusion techniques for diesel engine condition monitoring and fault diagnosis [13].

All the previously mentioned monitoring and diagnostic techniques have predominantly been implemented in large-type diesel engines such as marine two-stroke slow-speed engines, where the slow evolution of combustion event and high inertias of reciprocating and rotating masses facilitate the tracking of a faulty engine operating situation by either thermodynamic or mechanical cause. Also, most of the already published thermodynamic diagnostic studies have emphasized on the assessment of engine performance data without elucidating completely the effects of a faulty situation or engine component on the combustion mechanism. For this reason, in the present study an effort is made to shed light into the effect of specific faulty operating cases on the combustion mechanism and the pertinent performance characteristics of a small light-duty high-speed direct injection (DI) diesel engine. Specifically, it is theoretically examined the effect of faulty fuel injection system operation, which is modelled either as reduction of mean fuel injection pressure compared to its nominal value at a specific operating point or as reduction of fuel injected mass per engine cycle compared to its nominal value. Also, it is theoretically investigated the impact of faulty compression quality, which is modelled as reduction of compression ratio compared to its nominal value for the examined DI diesel engine. An engine closed-cycle simulation model is used to simulate the operation of a four-stroke high-speed DI diesel engine ("Lister LV1") under various mean injection pressures, fuel consumptions and compression ratios generating theoretical results for cylinder pressure, fuel evaporation rate and bulk gas temperature. Predicted cylinder pressure profiles are then supplied to a computational model developed in MATLAB under a diploma thesis conducted in Hellenic Naval Academy in order to perform a heat release rate analysis and to calculate main engine performance parameters. The evaluation of all theoretical results for combustion parameters and engine performance characteristics revealed that either the reduction of mean injection pressure or the reduction of compression ratio affected negatively the diesel engine combustion mechanism by delaying combustion initiation and, by increasing total combustion duration. The reduction of fuel injected mass per engine cycle resulted in significant reduction of engine power and efficiency due to reduction of engine supplied heating power whereas, it did not affect seriously commencement and the duration of the combustion event inside the combustion chamber.

DIESEL ENGINE DESCRIPTION

The diesel engine considered in the present study ("Lister LV1") is a four stroke, air cooled single-cylinder high-speed DI diesel engine, which is equipped with a bowl-in-piston. "Lister LV1" diesel engine has a cylinder bore of 0.08573m, a piston stroke of 0.08255 m and the connecting rod length is 0.1885m [14,15]. The compression ratio of "Lister LV1" diesel engine is 17:1 and its nominal speed range varies from 1000 to 3000 rpm. Diesel fuel is injected in "Lister LV1" engine through a three-hole injector (nozzle orifice diameter 250μm), which is located at the center of the combustion chamber and its opening pressure is 180 bar. "Lister LV1" engine is coupled with a Heenan & Froude hydraulic dynamometer at the premises of the Internal Combustion Engines Laboratory of National Technical University of Athens, Greece [14,15].

DESCRIPTION OF THE DIESEL ENGINE CLOSED-CYCLE SIMULATION MODEL

A two-dimensional multi-zone combustion model was used to simulate the physical and chemical phenomena that take place inside combustion chamber during closed cycle operation (intake and exhaust valves are closed). This model has been previously developed under a PhD thesis using the long-standing experience developed in the Laboratory of Internal Combustion Engines of National Technical University of Athens [16-20]. According to this model, the fuel jet coming out from each nozzle orifice during injection process is divided into distinctive control volumes, which are called "zones". Each fuel jet zone is treated as an open thermodynamic system, which exchanges energy and mass with its surroundings. The division of each fuel jet into zones allows the prediction of the temperature and the chemical composition of each zone at each crank angle integration step. In Figure 1 is given a representative schematic vies of the division of one fuel jet into zones at the axial and at the radial direction. It is given also in Figure 1 the effect of swirled air flow field on the formulation of the fuel jet shape [14,16-20].
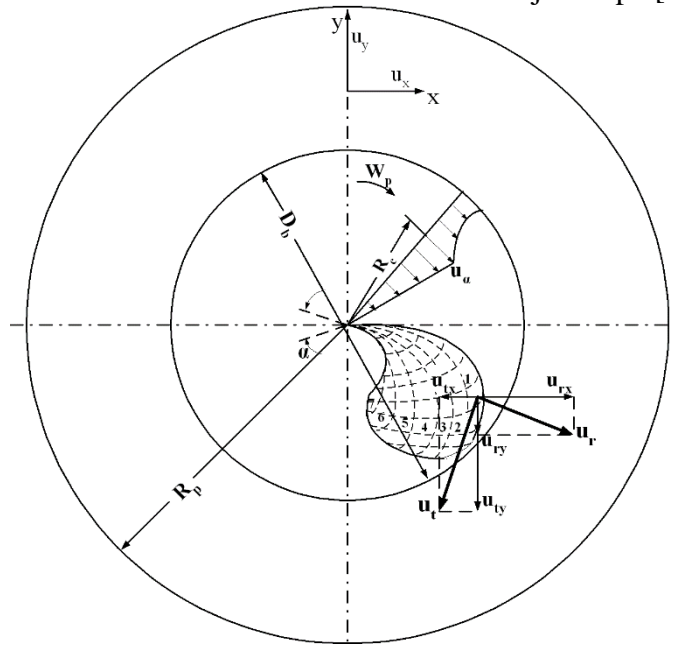

FIGURE 1. Schematic view of the swirled air flow field and one of the fuel jets on a plane perpendicular to the cylinder axis [14,19,20]

The thermodynamic conditions in each zone are calculated using the first law of thermodynamics and the mass and momentum conservation laws whereas the pressure inside the cylinder is considered uniform. Fuel jet zone temperature rate of variation depends directly from the energy released inside the zone due to the vaporized fuel and entrained air, zone heat losses, zone gas mixture internal energy and elementary technical work variation. Combining all these equations a final ordinary differential equation (ODE) is derived, which is numerically solved using a predictor – corrector scheme for predicting the cylinder pressure variation inside the cylinder. After numerically solving the ODE for cylinder pressure, several ODEs are also numerically solved using a predictor – corrector explicit method for predicting the instantaneous gas temperature inside each fuel jet zone [14,19,20].

Modeling of the Physical and Chemical Processes of the Four-Stroke Diesel Engine Closed Cycle

In-cylinder Heat Losses Modeling

The heat loss rate between the in-cylinder gas and the combustion chamber walls is calculated using the following relation [21]:

$$\dot{Q} = A\left[h\left(T_g - T_w\right) + c\sigma\left(T_g^4 - T_w^4\right) \right] \tag{1}$$

where:

- A is the instantaneous heat transfer area of the cylinder walls.
- Tw is the mean temperature of the cylinder walls, which is assumed to be invariable in space and time.
- σ is Stefan – Boltzmann constant
- c is a constant equal to 1.5.
- T_g is the bulk in-cylinder gas temperature at each crank angle step, which is predicted from the following equation:

$$T_g = \frac{\sum_{i=1}^{n+a} m_i c_{vi} T_i}{\sum_{i=1}^{n+a} m_i c_{vi}} \tag{2}$$

The first term in Eq. (1) corresponds to the heat losses of in-cylinder gas due to convection whereas, the second term in Eq. (1) corresponds to the radiation losses of the in-cylinder working medium. The instantaneous heat transfer rate calculated by Eq. (1) is distributed in fuel jet zones according to their individual temperature, mass and specific heat capacity as follows [22,23]:

$$\frac{d\dot{Q}_{i,w}}{d\varphi} = \dot{Q}\left(m_i c_{vi} T_i\right) \bigg/ \sum_{i=1}^{n+a} m_i c_{vi} T_i \tag{3}$$

Convection heat transfer coefficient h is given by the following relation assuming the existence of in-cylinder heat and fluid flow conditions like the ones of fully developed flow over a flat plate [24]:

$$h = c_h \, Re^{0.8} \, Pr^{0.33} \left(\lambda / \ell_{char}\right) \tag{4}$$

where Re is the dimensionless Reynolds number, Pr is the dimensionless Prandtl number, λ is the thermal conductivity of the in-cylinder gaseous medium and ℓ_{char} is the characteristic length. The characteristic mean velocity of the in-cylinder bulk gas used for the calculation of the Reynolds number is given by:

$$\bar{u} = \left(u^2 + u_T^2 + u_p^2\right)^{0.5} \tag{5}$$

where u_p is the instantaneous piston velocity, which is a function of cylinder geometrical dimensions [1]. Reynolds and Prandtl numbers are calculated as follows:

$$Re = \frac{\bar{u} \ell_{char} \rho}{\mu}, \quad Pr = \frac{\mu c_p}{\lambda} \tag{6}$$

A dimensionless turbulent kinetic energy (k-ε) model is used for the prediction of u and u_T velocities [25].

Air Swirl Model – Prediction of Intake Air Angular Velocity

Air angular velocity inside the combustion chamber is calculated by solving the angular momentum conservation law. It should be noted here, that in many cases, intake air is inducted in the engine combustion chamber with angular momentum as a result of its rotation around cylinder vertical axis. This motion of the intake air is called "Swirl" and it is usually in small-bore diesel engines, which are equipped with bowl-in-piston. Swirl motion is applied to prevent the fuel jet impingement to the bowl-in-piston walls and thus, to avoid the temporarily cooling of impinged fuel due to its heat loss to piston bowl walls. In most of the cases, the amount of impinged fuel cannot be burned completely enhancing thus, the formation rate of unburned hydrocarbons. In general, intake air swirled induction inside the cylinder promotes air entrainment inside fuel jet improving thus, local fuel-air mixing.

The solution of the angular momentum conservation equation requires the knowledge of the swirled intake air tangential velocity. Hence, it is assumed that the tangential intake air profile on a plane perpendicular to the cylinder longitudinal axis is a hybrid scheme comprised of a solid core, which is surrounded by a flow field. This hybrid scheme considers the air viscosity, which creates a boundary layer close to the combustion chamber walls [26]. The tangential air velocity profile is given by the following relation [1]:

$$\left.\begin{array}{ll} u_t = W_p R & \gamma\iota\alpha\ 0 \le R \le R_c \\ u_t = W_p R_c \left(R_c / R \right)^n & \gamma\iota\alpha\ R_c \le R \le R_p \end{array}\right\} \tag{7}$$

where u_t is the tangential air velocity, W_p is the angular air velocity, n is an exponent which varies from 0 to 0.1 and R_c is the air solid core rotation radius, which is calculated as follows:

$$R_c = R_m \left(D_b / 2 R_p \right) \tag{8}$$

Consequently, for a given combustion chamber geometry and known angular air velocity W_p, the tangential air velocity profile can be calculated using Eqs (7) and (8).

For the calculation of the angular air velocity W_p, a simple scheme of "air solid core rotation" is used, where the angular momentum conservation equation is applied for the combustion chamber gaseous content [27]. The value of air angular velocity when the intake valve is closed corresponds to the initial value of air angular velocity and it is an input value of the closed-cycle simulation model expressed as the ratio of air angular velocity to the engine rotational speed (i.e. swirl ratio). This value is obtained from relevant experimental data. The conservation law of angular momentum in differential form is given by:

$$\frac{d(IW)}{dt} = I \frac{dW}{dt} + W \frac{dI}{dt} = -M_r \tag{9}$$

The rotating moment of inertia I of the in-cylinder gas is calculated as follows:

$$I = \frac{1}{2} m_a \frac{R_p^2 S_p + \left(D_b / 2 \right)^4 S_b}{R_p^2 S_p + \left(D_b / 2 \right)^2 S_b} \tag{10}$$

where m_a is the mass of the trapped in-cylinder gas. The resulting rotating torque M_r, which act on the fluid is:

$$M_r = M_{cyl} + M_{p-c} \tag{11}$$

where M_{cyl} is the resistance torque to the in-cylinder fluid flow due to its contact with combustion chamber walls and M_{p-c} is the generating torque due to the friction of the in-cylinder gas with the piston crown and the cylinder head. Fluid resistance torque is given by the expression:

$$M_{cyl} = \tau_{cyl} A_{cyl} R_p = \left(\frac{1}{2} f_{cyl} \rho_a u_{tRp}^2 \right) 2\pi R_p^2 S_p \tag{12}$$

Where u_{tRp} is the tangential air velocity at radius R_p, which, according to Eq (7), is calculated as follows:

$$u_{tRp} = W_p R_c \left(R_c / R_p \right)^n \tag{13}$$

Combining Eqs (12) and (13) it is finally obtained:

$$M_{cyl} = f_{cyl} \pi W_p^2 R_p^2 R_c^2 \left(R_c / R_p \right)^{2n} S_p \tag{14}$$

Friction coefficient f_{cyl} of the in-cylinder gas motion is calculated assuming again the same conditions with the ones of the fully developed fluid flow over a flat plate:

$$f_{cyl} = 0.058 \, Re^{-0.2} \tag{15}$$

The cylinder bore (equal to $2R_p$) and the air velocity u_{tRp} are used as characteristic length and as characteristic velocity respectively to calculated Reynolds number. The rotating torque due to air friction at the piston top head and at the cylinder head is assumed that it acts on the cylinder mean radius ($R_p/2$) and that it is the same with the one calculated as fluid friction between two flat plates. According to this assumption, the torque M_{p-c} is calculated using the following equation [1]:

$$M_{p-c} = 2\left(\tau_{p-c} A_{p-c} R_p / 2 \right) = \left(\frac{1}{2} f_{p-c} \rho_a u_{tRp/2}^2 \right) \pi R_p^3 \tag{16}$$

where $u_{tRp/2}$ is the tangential air velocity at radius $R_p/2$, which is calculated as follows:

$$u_{tRp/2} = W_p \left(R_p / 2 \right) \tag{17}$$

Finally, the generating torque M_{p-c} due to the friction of the in-cylinder gas with the piston crown and with the cylinder head is estimated according to the following relation:

$$M_{p-c} = f_{p-c} \pi \rho_a W_p^2 \left(R_p^5 / 8 \right) \tag{18}$$

Friction coefficient f_{p-c} is calculated from Eq. (15) using radius R_p as characteristic length and air velocity $u_{tRp/2}$ for the calculation of the pertinent Reynolds number.

Fuel Jet Development Model

Fuel injected mass per crank angle integration step is divided into n_r zones through fuel jet, where n_r is an odd number. Hence, fuel jet zones are arranged proportionally on either side of the

longitudinal axis of the fuel jet. Fuel injected mass m_f per engine cycle is distributed into zones as follows [14,16-18,20]:

$$m_{f,i} = \frac{A_{ho,i}}{A_{ho}} m_f \tag{19}$$

Where $A_{ho,i}$ is a predefined portion of the total injector nozzle area A_{ho}. At next, as a certain crank angle degree step $\Delta\varphi$ has passed from the beginning of the fuel injection process, a new group of "n" fuel jet zones if formed following the same path as previously described. This process is continued until the completion of the fuel injection process. The axial velocity of each fuel jet zone is calculated by adopting the following semi-empirical relation [14,16-18,20]:

$$\begin{cases} \dfrac{u_{x,i}}{u_{inj}} = \left(\dfrac{\Delta X_0}{\Delta X_{x,i}}\right)^{n_1}, & \gamma\iota\alpha \; \Delta X_{x,i} > 6.57 d_{ho} = \Delta X_0 \\ u_{x,i} = u_0, & \gamma\iota\alpha \; \Delta X_{x,i} \leq 6.57 d_{ho} \end{cases} \tag{20}$$

where $i = 1$ and $i = n_r$ represent the leading and the trailing zone respectively. A linear distribution with respect to number of radial jet zones is used for the calculation of exponent n_i, which varies from 0.7 to 0.9 from the internal to the external zones. The initial value of the radial component of the fuel jet velocity is estimated as follows:

$$u_{r,i} = u_{inj} \tan\left(\frac{\theta_0}{r_0} r_i\right) \tag{21}$$

where r_0 is the radius of the injector nozzle as presented in Figure 2 and r_i is the radial distance of fuel jet zone "i" from the central lines.
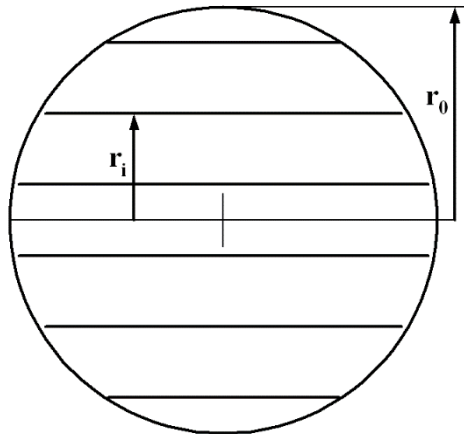

FIGURE 2. Fuel jet distribution into radial zones [14,20]

The fuel jet cone angle at the exit of the injector nozzle is calculated using the following relation [1,28]:

$$\theta_0 = 0.05 \left(\frac{d_{inj}^2 \rho_a \Delta P}{\mu_a^2}\right)^{0.25} \tag{22}$$

The local fuel jet cone angle is calculated afterwards from the fuel jet geometry as it results from the local radial and axial velocities of the external fuel jet zones. Calculating the local air velocity components in both radial and axial directions and using the momentum conservation

equations in both axes, the effect of air swirl on fuel jet geometry can be considered. From the procedure it results that the axial fuel jet penetration is reduced leading to a rapid deceleration of the fuel jet and thus, to the increase of the air entrainment rate. Due to air swirl inside the combustion chamber, fuel jet zones deviate from the initial direction and as result an increase of air entrainment rate is observed inside fuel jet zones. Fuel jet zone deviation from the initial direction is calculated considering local air velocities as follows:

$$\left.\begin{aligned} u_{tx,i} &= u_{x,i} + u_t \, sin(\theta_i) \\ u_{tr,i} &= u_{r,i} - u_t \, cos(\theta_i) \end{aligned}\right\} \tag{23}$$

Where u_t is the local air swirl velocity and θ_i is the angular position of each fuel jet zone inside the combustion chamber. The above-mentioned equations are implemented for the cases before and after the fuel jet impingement to the combustion chamber walls. The well-tested theory of Glauert for the interaction of fuel jet and combustion chamber walls [29,30] is used for the determination of the time evolution of the fuel jet zones after the jet impingement to the combustion chamber walls. According to this theory, fuel jet zone velocity after impingement is given by the following equation:

$$w_i = w_{0,i} \left(\frac{r_{0,i}}{r_i} \right) \tag{24}$$

Where $r_{0,i}$ is the initial radial zone position with respect to the jet axis after impingement and $w_{0,i}$ is the initial velocity. It is assumed that the fuel jet zone follows a path alongside the combustion chamber walls, where its radial distance "δ" from the wall determines the thickness of the fuel jet boundary layer on the combustion chamber wall and is given from the relation [22,23,29]:

$$\delta_i = \delta_{0,i} \left(\frac{r_i}{r_{0,i}} \right) \tag{25}$$

where $\delta_{0,i}$ is the initial zone distance from the combustion chamber wall after the impingement. Before the jet impingement the velocities are divided into two components: One perpendicular and one parallel to the combustion chamber walls. After this, the part of fuel jet zone, which corresponds to the parallel velocity deviates completely whereas, the perpendicular part of zone is divided into two parts: The right and left part. Hence, the zone part, which has velocity opposite to the parallel velocity component is considered to create a new zone. The initial values for $w_{0,i}$ and $\delta_{0,i}$ are determined by applying the mass and the energy conservation laws taking also into consideration the local fuel jet geometry [22].

Air entrainment rate into zones is determined using the momentum conservation law for the injected fuel. Air entrainment rate is obtained from the following expression [28,31]:

$$m_f u_{inj} = (m_f + m_a)u \tag{26}$$

The left-side part of the previous equation is equal to the initial zone momentum whereas, the right-side part corresponds to the zone momentum after time "t". Differentiating both sides of the previous equation is obtained the following differential equation for the air entrainment rate:

$$u \frac{dm_a}{dt} = -(m_a + m_f) \frac{du}{dt} \tag{27}$$

Hence, having given the instantaneous total air mass entrained into zones from the beginning, is calculated the air entrainment rate at each integration crank angle degree step. It should be mentioned that the entrained air into fuel zones results in their deceleration.

Fuel Atomization Model

Inside each fuel jet zone, fuel is split into packages (i.e. groups), in which all fuel droplets have the same "Mean Sauter Diameter – SMD". The "Mean Sauter Diameter (D_{SM}) is obtained from the following semi-empirical relation, which has been derived from experimental data analysis [31]:

$$D_{SM,1} = 0.38 \, Re_{inj}^{0.25} \, We_{inj}^{-0.32} \left(\frac{v_l}{v_a} \right)^{0.37} \left(\frac{\rho_l}{\rho_a} \right)^{-0.47} d_{inj}$$

$$D_{SM,2} = 4.12 \, Re_{inj}^{0.12} \, We_{inj}^{-0.75} \left(\frac{v_l}{v_a} \right)^{0.54} \left(\frac{\rho_l}{\rho_a} \right)^{0.18} d_{inj}$$

(28)

Where the indices "1" and "2" denote complete and incomplete fuel jets respectively. In the previous relation, We is the dimensionless Weber number, v_l, ρ_l are the kinematic viscosity and the density of the liquid fuel droplet, v_α, ρ_α are the kinematic viscosity and the density of the surrounding air and d_{inj} is the injector nozzle orifice diameter. The mean droplet dimeter is obtained as the maximum of these two values. By this modelling approach is taken into consideration the effect of fuel physical properties.

Fuel Vaporization Model

The well-known model of Borman and Johnson [32] is used for the modeling of the vaporization process of the liquid fuel inside each jet zone. This model succeeds in describing effectively the fuel vaporization phenomenon taking into consideration the coupled heat and mass transport phenomena that take place at the fuel droplet – air interface. According to the model of Borman and Johnson the reduction rate of a fuel droplet radius due to vaporization is given by the following relation:

$$\frac{dr}{dt} = -\frac{\rho_a}{\rho_l} \frac{D_{af}}{2r} Sh \, ln \left[1 + \left(\frac{y_s - y}{1 - y_s} \right) \right]$$

(29)

where:
- ρ_α is the air density in kg/m^3.
- ρ_l is liquid fuel density in kg/m^3.
- $D_{\alpha f}$ is the liquid diffusion coefficient to the gas phase in m^2/s.
- r is the fuel droplet radius in m.
- y is the fuel mass concentration of the gas phase zone around the droplet.
- y_s is the fuel mass concentration at the droplet surface, which is calculated as follows:

$$y_s = \frac{MB_f \, p_{vp}}{MB_f \, p_{vp} + MB_a \left(p - p_{vp} \right)}$$

(30)

where:

- MB_f is the fuel molecular weight.
- MB_a is the air molecular weight.
- p is the in-cylinder pressure at each crank angle degree integration step.
- p_{vp} is the fuel vapor pressure, which at the droplet surface is considered equal to the corresponding fuel partial pressure.

It should be mentioned that analytical correlations based on experimental data for the n-dodecene ($C_{12}H_{24}$) were used for the calculation of the liquid fuel thermophysical properties [14].

The energy balance between liquid droplet and surrounding air taking into consideration the latent heating of the liquid droplet and its mass reduction due to evaporation is expressed as follows [32,33]:

$$m_l c_{pl} \frac{dT_l}{dt} - 4\pi r^2 \rho_l \Delta h_v \frac{dr}{dt} = 4\pi r^2 \dot{q} \tag{31}$$

The first term of the Eq. (31) express the required heat for the droplet sensible heating and is becomes zero when the droplet temperature becomes equal to saturation temperature T_s. The second term of the Eq, (31) expresses the latent heat of vaporization. This means that droplet temperature remains constant and equal to saturation temperature T_s. The second part of the Eq. (31) expresses the total heat, which is offered from the droplet surrounding environment (gaseous mixture of surrounding air and gaseous fuel) for its heating and evaporation. It is assumed that all fuel droplets of each jet zone (at the time instant each jet zone is injected) have initially the same diameter equal to the Sauter Mean Diameter (SMD). Each jet zone fuel evaporation rate relates to fuel droplet evaporation rate as follows [16,18]:

$$\frac{dm_{ev,i}}{dt} = N_{d,i} \frac{dm_{ev,d,i}}{dt} \tag{32}$$

where the index "i" denotes the increasing zone number, the index d refers to droplet whereas, $N_{d,i}$ is the number of droplets of fuel jet zone "i". Hence, fuel jet zone evaporation rate is calculated as follows:

$$\frac{dm_{ev,i}}{dt} = N_{d,i} \left[2\pi\rho_a D_{af} Sh \, ln \left[1 + \left(\frac{y_s - y}{1 - y_s} \right) \right] \right]_i \tag{33}$$

The heat flux $\dot{q}$ absorbed by each droplet is calculated according to the following relation:

$$\dot{q} = \frac{\lambda_a (T - T_l)}{2r} Nu \frac{ln \left[1 + \left(\frac{y_s - y}{1 - y_s} \right) \right]}{\left(\frac{y_s - y}{1 - y_s} \right)} \tag{34}$$

Hence, the total amount of heat offered to fuel jet zone "i" for its heating and evaporation is:

$$\frac{d\dot{Q}_{ev,tot,i}}{dt} = N_{d,i} \left(4\pi r^2 \dot{q} \right) \tag{35}$$

Consolidating all above-mentioned information, the total fuel evaporation rate is:

$$\frac{dm_{ev,tot}}{dt} = \sum_{i=1}^{n} \frac{dm_{ev,i}}{dt} \qquad (36)$$

Integrating Eqs (29), (31) and (33) for each zone it is calculated the droplet radius, the droplet temperature, which is equal to jet zone fuel temperature, and the fuel evaporated mass. Calculated droplet temperature T_1 is further used for the prediction of the mean temperature T_m of the gaseous film, which is formed during evaporation around each droplet [16,18,33]:

$$T_m = \frac{T_a + 2T_l}{3} \qquad (37)$$

Temperature T_m is the temperature used for the calculation of the thermophysical properties of the gaseous mixture formed due to fuel evaporation around the droplet. Regarding the total heat supplied to the liquid fuel of each jet zone, it is considered that is partially attributed to the jet zone itself and partially to fuel jet surrounding air as follows [16,18]:

$$\frac{d\dot{Q}_{ev,tot,i}}{dt} = \frac{d\dot{Q}_{ev,i}}{dt} + \frac{d\dot{Q}_{ev,a,i}}{dt} \qquad (38)$$

where the index "α" denotes the air zone. The contribution of each zone $d\dot{Q}_{ev,i}$ and the corresponding contribution of jet surrounding air $d\dot{Q}_{ev,a,i}$ to the total evaporation heat supplied to each jet zone $d\dot{Q}_{ev,tot,i}$ is determined by the following relation:

$$\left.\begin{aligned}
\frac{d\dot{Q}_{ev,i}}{dt} &= \frac{m_l T_l}{m_l T_l + m_a T_a} \frac{d\dot{Q}_{ev,tot,i}}{dt} \\
\frac{d\dot{Q}_{ev,a,i}}{dt} &= \frac{m_a T_a}{m_l T_l + m_a T_a} \frac{d\dot{Q}_{ev,tot,i}}{dt}
\end{aligned}\right\} \qquad (39)$$

Ignition Delay Model

For the calculation of the ignition delay the following relation was used, which has been proposed by Assanis et al. [34] and it takes into consideration the value of the local fuel/air equivalence ratio Φ inside the combustion chamber:

$$S_{pr} = \int_{0}^{1} \frac{1}{a_{del} p_g^{-2.5} \Phi_{eq}^{-1.04} \exp\left(5000/T_g\right)} dt \qquad (40)$$

where "Φ_{eq}" is the local fuel/air equivalence ratio, T_g is the local gas temperature and p_g is the in-cylinder pressure. Fuel is ignited locally in the jet zone, where the integral of Eq. (40) becomes equal to unity and the time interval between fuel injection timing angle and ignition angle is considered as ignition delay. The selection of this ignition delay model was made since it takes into consideration the local fuel/air equivalence ratio, the local zone temperature and the in-cylinder pressure.

Combustion Rate Prediction Model

The mathematical model used for the prediction of fuel combustion rate takes into consideration the local stoichiometric fuel/air ratio and the local temperature. This model is literally an Arrhenius relationship, which includes the cylinder pressure, the local zone
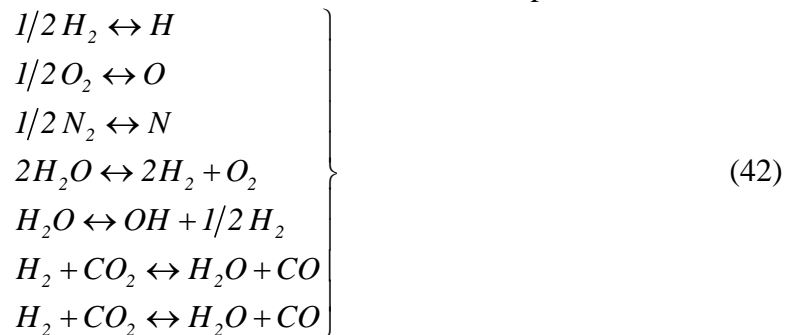
temperature and the local fuel availability with respect to entrained air in each zone. Hence, according to the model of Hodgetts and Shroff [35], the premixed combustion rate is given by the following relation:

$$\frac{dm_{bu,i}}{dt} = c_{bu} p^{0.757} \exp\left(-\frac{4500}{T_i}\right) \times \min\left[m_{f,ev,i}, m_{a,av,i} FA_{st}\right] \qquad (41)$$

The term $\min\left[m_{f,ev,i}, m_{a,av,i} FA_{st}\right]$ denotes the dependence of the premixed combustion rate from the fuel vapor and the available entrained air in each jet zone. Equation (41) is implemented for each jet zone and it is numerically integrated for the derivation of the local premixed combustion rate. The model of Eq. (41) is not used for the prediction of diffusion combustion rate since this rate is controlled by the air entrainment rate in each fuel jet zone.

Combustion Products Dissociation – Chemical Equilibrium Scheme

It is well known that due to high in-cylinder temperatures the products of perfect combustion are further dissociating to a number of species, which in most cases is limited to the following 11 ones: N_2, O_2, CO_2, H_2O, CO, H_2, NO, OH, N, H, O [36-40]. Chemical equilibrium reactions, which describe the formation of the above-mentioned eleven dissociation species are [37]:

$$\left.\begin{array}{l} 1/2\,H_2 \leftrightarrow H \\ 1/2\,O_2 \leftrightarrow O \\ 1/2\,N_2 \leftrightarrow N \\ 2H_2O \leftrightarrow 2H_2 + O_2 \\ H_2O \leftrightarrow OH + 1/2\,H_2 \\ H_2 + CO_2 \leftrightarrow H_2O + CO \\ H_2 + CO_2 \leftrightarrow H_2O + CO \end{array}\right\} \qquad (42)$$

where K_{pir} are the equilibrium constants (ir = 1, 2, … ,7). Various approaches have been proposed in the literature for the numerical solution of the chemical equilibrium equations [36-40]. The common reference point of all numerical methods is the derivation of a non linear 11 x 11 system for the equilibrium concentration of the above-mentioned species using the definition equations of chemical equilibrium constants of the 7 above-mentioned reactions and the C, H, O and N balances between perfect combustion reactants and products. The numerical methods proposed for the solution of the above-mentioned chemical equilibrium scheme differ in terms of the numerical method used for the solution of the non linear algebraic system. In the present study the numerical method of Olikara and Borman [39] was used for the solution of chemical equilibrium equations in each modified version for the 11 species as it was suggested by Rakopoulos et al. [37].

BRIEF DESCRIPTION OF MATLAB MODEL USED FOR HEAT RELEASE RATE ANALYSIS AND FOR THE CALCULATION OF ENGINE COMBUSTION AND PERFORMANCE CHARACTERISTICS

A computational model was developed in MATLAB under a diploma thesis performed in Hellenic Naval Academy for performing heat release rate analysis and for calculating the main

combustion and performance characteristics of the examined diesel engine under varying injection pressure, fuel consumption and compression ratio. The specific model was initially developed for processing raw experimental data for cylinder pressure, injection pressure and TDC position from an experimental diesel engine under various operating conditions and for deriving the mean cylinder pressure and mean injection pressure profile. In the present study the developed MATLAB model was modified in order to use the cylinder pressure profiles generated by the closed-cycle simulation model (i.e. multi-zone combustion model) for different mean injection pressures, engine fueling rates and compression ratios for performing a heat release rate analysis and for calculating the main combustion and performance characteristics of the examined experimental diesel engine. The heat release rate analysis performed by the developed MATLAB model is based on the combination of the first law of thermodynamics for a closed thermodynamic system and the ideal gas equation of state for deriving gross and net heat release rates considering instantaneous in-cylinder gas heat losses, which were calculated using the well-known Annand's heat transfer model. In addition, the MATLAB model calculates the main combustion and performance characteristics of the examined experimental diesel engine such as indicated power, Indicated Specific Fuel Consumption (ISFC), peak cylinder pressure, ignition delay, ignition angle and the combustion durations corresponding to 5%, 25%, 50% and 90% of injected fuel mass burned.

TEST CASES EXAMINED

To examine the effect of the faults related to injection and compression quality the following cases were considered:

- Reduction of injection pressure compared to the nominal value: This investigation was performed to examine the effect of reduced – compared to the nominal injection pressure value, which satisfies the experimental values of cylinder pressure – injection pressure, which appears when for example the fuel injector or the high pressure fuel pump faults and as result the fuel is injected inside the cylinder with lower pressure compared to the one specified for the specific engine operation point. In this case the multi-zone combustion model was used top generate a theoretical cylinder pressure profile for the nominal value of fuel injection pressure i.e. 240 bars. This value of fuel injection pressure is considered during cylinder pressure calibration procedure in order the predicted cylinder pressure data to match experimental cylinder pressure data at 2500 rpm and at 80% of full engine load. The multi-zone combustion model was also used to generate cylinder pressure profiles for the cases of 216 bars, 192 bars and 168 bars fuel injection pressure, which correspond to 90%, 80% and 70% of the fuel injection pressure considered i.e. 240 bars to match experimental cylinder pressure data at 2500 rpm and at 80% of full engine load.

- Variation of total fuel injected quantity per engine cycle i.e. variation of engine fuel consumption: This investigation is performed to examine the effect of variable fuel consumption when for example the injector nozzle orifice has been blocked or the injector nozzle needle has been stacked and as result the fuel injector does not inject the proper fuel quantity per engine cycle. In this case also the multi-zone combustion model was used to generate theoretical cylinder pressure profile for the proper fuel injected quantity per engine cycle i.e. 1.1 kg/h (nominal value at 2500 rpm and at 80% of full load). This value of fuel consumption is not the experimental one, which corresponds exactly to engine operation at 2500 rpm and at 80% of full load but it is the theoretical fuel consumption which provides a

theoretical cylinder profile which matches with the experimental one at this operating case. Additional cylinder pressure profiles were generated using the multi-zone model for values of fuel consumption equal to 1.265 kg/h (115% of the nominal value), 0.99 kg/h (90% of the nominal value) and 0.88 kg/h (80% of the nominal value). The case of 1.265 kg/h is examined to simulate the case when the power of one engine cylinder is higher than the standard one due to excess fuel injected quantity per engine cycle.

- Reduction of compression ratio (CR) due to potentially excessive wear of piston compression rings: The wear of compression rings due to either erosive environment as a result of the fuel oil composition or due to excessive in-cylinder gas temperature results in reduction of the effective compression ratio and results in increased blow-by losses to engine crankcase. The multi-zone combustion model was used also in this case to predict cylinder pressure profile at 2500 rpm and at 80% of full load using a nominal value of CR equal to 17.1:1. This cylinder pressure profile was compared with the corresponding experimentally obtained cylinder pressure profile. Afterwards, the multi-zone combustion model was used to generate cylinder pressure profiles for the three different values of CR namely 16.67:1, 16.25:1 and 15.39:1, which correspond to 97.5%, 95% and 90% of the nominal CR value.

RESULTS AND DISCUSSION

Experimental Assessment of the Diesel Engine Closed-Cycle Simulation Model Predictive Ability

Before the implementation of the theoretical investigation for the examination of the effect of variable injection pressure, fuel consumption and compression ratio on the combustion and performance characteristics of the single-cylinder DI diesel engine "Lister LV1" the ability of the multi-zone combustion model to predict with enough accuracy the cylinder pressure profile should be assessed. For this reason, in Figure 3 is shown a comparison of predicted and experimental cylinder pressure data at 2500 rpm and at 80% of full load. The predicted cylinder pressure values have been generated using the multi-zone combustion model for mean injection pressure equal to 240 bar, fuel consumption equal to 1.1 kg/h, compression ratio equal to 17.1:1 and injection timing equal to 15 degrees before TDC. As evidenced from Figure 3, the multi-zone combustion model succeeds to predict with enough accuracy the measured cylinder pressure both during compression and during combustion and expansion stroke. Hence, it can be assumed with adequate confidence that the predictions for cylinder pressure of the multi-zone combustion model when the mean injection pressure or the fuel consumption or the compression ratio are varying are trustworthy.
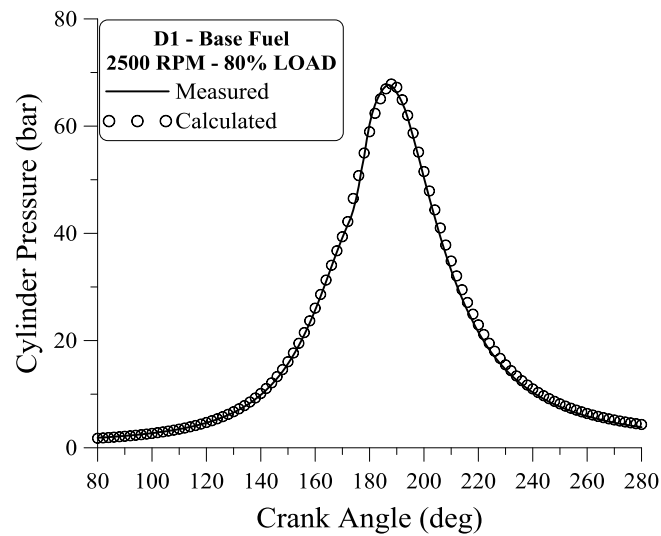
FIGURE 3. Comparison of theoretical and experimental values of cylinder pressure of "Lister LV1" engine at 2500 rpm and at 80% of full load

Effect of Mean Injection Pressure Variation on DI Diesel Engine Performance and Combustion Characteristics

In this paragraph is examined the effect of mean injection pressure variation on the performance parameters and the combustion characteristics of a four-stroke high-speed single-cylinder DI diesel engine "Lister LV1". More specifically, it is examined the reduction of mean injection pressure compared to its nominal value at 2500 rpm and at 80% of full load for simulating the injection pressure loss when for example the fuel pump does not provide enough compression of the injected fuel. In such case fuel injector needle is lifted at the proper crank angle (i.e. proper injection timing) and the proper fuel quantity is injected at a specific engine speed and load, but fuel injection is not performed with the proper injection pressure due to fuel pump problems such as increased blow-by losses of the reciprocating fuel pump. Hence, it is examined the effect of variable mean injection pressure compared to its nominal value (this value corresponds to the mean injection pressure which provides a theoretical cylinder pressure profile that matches with the corresponding experimental one) to cylinder pressure profile, indicated power, ISFC, instantaneous and cumulative net heat release rate, instantaneous heat loss rate, ignition angle, ignition delay and combustion durations of 5%, 25%, 50% and 90% of total fuel injected quantity per engine cycle.

The values of mean injection pressure examined in the present study are:

- 240 bar – Nominal value of mean injection pressure, which provides a theoretical cylinder pressure profile using the multi-zone combustion model that matches the corresponding experimental cylinder pressure profile at 2500 rpm and at 80% load.
- 216 bar – This value of mean injection pressure corresponds to the 90% of the nominal value.
- 192 bar – This value of mean injection pressure corresponds to the 80% of the nominal value.
- 168 bar - This value of mean injection pressure corresponds to the 70% of the nominal value.

For each one of the above-mentioned mean injection pressures are derived theoretical cylinder pressure profiles using the multi-zone combustion model. It should be mentioned that the fuel injection process in the closed-cycle simulation model is modelled as a rectangular pulse of injection pressure. This means that for the time duration the injector needle is open the fuel injection pressure is constant and equal to its mean value, which is provided to the closed-cycle simulation model as input. Hence, initially a simulation was performed at 2500 rpm and at 80% of full load using mean injection pressure value equal to 240 bar, fuel consumption equal to 1.1 kg/h, compression ratio equal to 17.1:1 and injection timing equal to 15 degCA BTDC. At all other cases of mean injection pressure, the above-mentioned input values of fuel consumption, compression ratio and injection timing remained the same to isolate only the effect of mean injection pressure. Afterwards, the theoretical cylinder pressure profiles derived from the previous computational investigation were supplied to the MATLAB model for performing a heat release rate analysis and for predicting the main combustion parameters and engine performance characteristics at each injection pressure case.

In Figure 4(a) is shown the impact of mean injection pressure reduction on the predicted instantaneous fuel evaporation rate. Specifically, in Figure 4(a) are provided theoretical results for fuel evaporation rate for four values of mean injection pressure i.e. 240 bar, which corresponds to the nominal value of mean injection pressure at 2500 rpm and at 80% load, 216 bar, 192 bar and 168 bar. As witnessed from Figure 4(a), the reduction of mean injection pressure from 240 bar to 168 bar results in reduction of the peak values of fuel evaporation rate and results in elongation of the fuel evaporation process. Hence, the reduction of mean injection pressure results in direct reduction of the velocity of the fuel injected spray at the exit of the injector nozzle and thus, results in significant reduction of the vaporized fuel mass per crank angle degree step. The considerable reduction of fuel evaporation rate results in the significant increase of the fuel evaporation process duration since the total fuel injected quantity remains the same at all cases of fuel injection pressure.

In Figure 4(b) is shown the effect of mean injection pressure variation on the predicted cylinder pressure profiles. Specifically, in Figure 4(b) are given theoretical results for cylinder pressure for four values of mean injection pressure i.e. 240 bar, which corresponds to the nominal value of mean injection pressure at 2500 rpm and at 80% load, 216 bar, 192 bar and 168 bar. As evidenced from Figure 4(b), the reduction of mean injection pressure from 240 bar to 168 bar results in reduction of cylinder pressure around TDC and thus, in significant reduction of peak cylinder pressure. The reduction of mean injection pressure did not affect the cylinder pressure increase during compression stroke whereas, the impact of mean injection pressure reduction on cylinder pressure during expansion stroke is imperceptible. The reduction of cylinder pressure around TDC with decreasing mean injection pressure can be attributed to the reduction of fuel evaporation rate as evidenced in Figure 6(a), which results in reduction of fuel combustion rate during injection process curtailing thus, cylinder pressure around TDC.

The impact of mean injection pressure reduction on predicted in-cylinder bulk gas temperature is shown in Figure 4(c). More specifically, in Figure 4(c) are given theoretical results for bulk gas temperature for four values of mean injection pressure i.e. 240 bar, which corresponds to the nominal value of mean injection pressure at 2500 rpm and at 80% load, 216 bar, 192 bar and 168 bar. As evidenced from Figure 4(c), the reduction of mean injection pressure results in noticeable reduction of in-cylinder bulk gas temperature around TDC as a result of the corresponding reduction of in-cylinder pressure witnessed in Figure 4(b). The effect of mean injection pressure reduction on in-cylinder bulk gas temperature during expansion stroke is rather imperceptible.
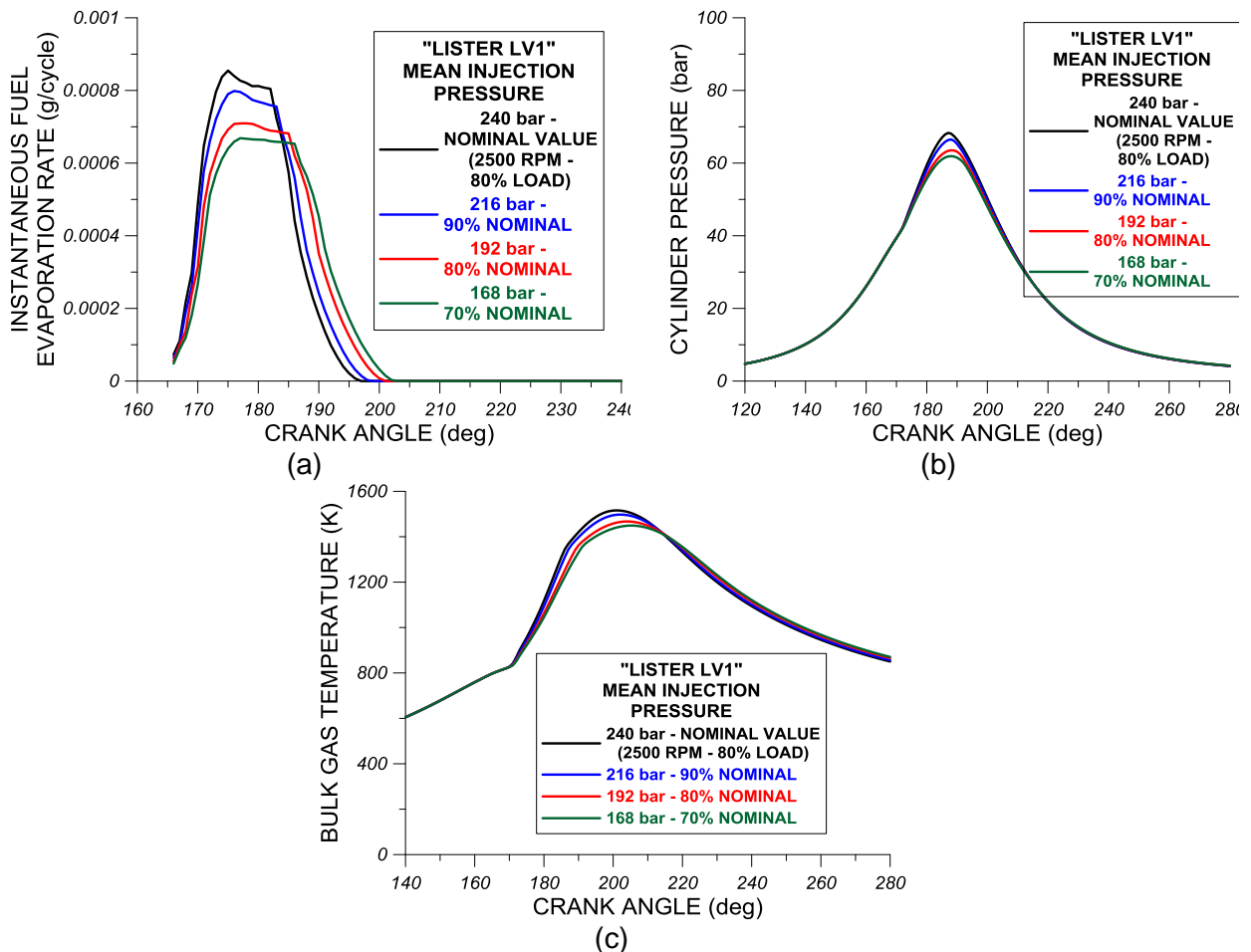
FIGURE 4. Effect of fuel mean injection pressure reduction on theoretical (a) instantaneous fuel evaporation rate, (b) cylinder pressure and (c) in-cylinder bulk gas temperature profiles of "Lister LV1" engine. Theoretical results are presented at 240 bars (nominal value of injection pressure), 216 bars (90% of nominal value of injection pressure), 192 bars (80% of nominal value of injection pressure) and 168 bars (70% of nominal value of injection pressure) of fuel injection pressure. The fueling rate of 1.1 kg/h, 240 bars fuel injection pressure and 17.1:1 compression ratio corresponds to "Lister LV1" engine operation at 2500 rpm and at 80% of full load.

Figure 5 depicts the effect of mean injection pressure variation on calculated instantaneous net heat release rate (Figure 5(a)), instantaneous heat losses rate (Figure 5(b)) and cumulative net heat release rate (Figure 5(c)). Specifically, in Figure 5(a) is shown instantaneous net heat release rate profiles for the following four values of mean injection pressure i.e. 240 bar, which corresponds to theoretical engine operation at 2500 rpm and at 80% load, 216 bar, 192 bar and 168 bar. As evidenced from Figure 5(a), the reduction of injection pressure results in the reduction of premixed combustion phase intensity leading thus, to lower peak premixed net heat release rates. On the other hand, the reduction of mean injection pressure promotes diffusion-controlled combustion phase. Hence, overall it can be stated that the reduction of mean injection pressure for the same fuel injected mass per engine cycle results in reduction of the fuel burned under premixed conditions and in parallel results in the increase of the fuel percentage burned

under diffusion-controlled conditions. This is attributed to the curtailment of fuel evaporation rate with decreasing mean injection pressure, which results in reduction of fuel percentage burned under premixed conditions and shifts the fuel combustion towards diffusion-controlled phase leading thus, to the deterioration of soot emissions primarily generated under diffusion-combustion conditions. From the observation of Figure 5(b), it can be stated that the reduction of mean injection pressure results in reduction of instantaneous heat losses rate during initial stages of expansion stroke and specifically from almost 180 degrees ABDC until 210 degrees ABDC as a main outcome of the corresponding reduction of bulk gas temperature evidenced in Figure 4(c). According to Figure 5(c), the reduction of mean injection pressure results in reduction of cumulative net heat release rate during expansion stroke and specifically, from 175 degrees ABDC until almost 220 degrees ABDC as a result mainly of the variations observed in instantaneous net heat release rate in Figure 5(a).
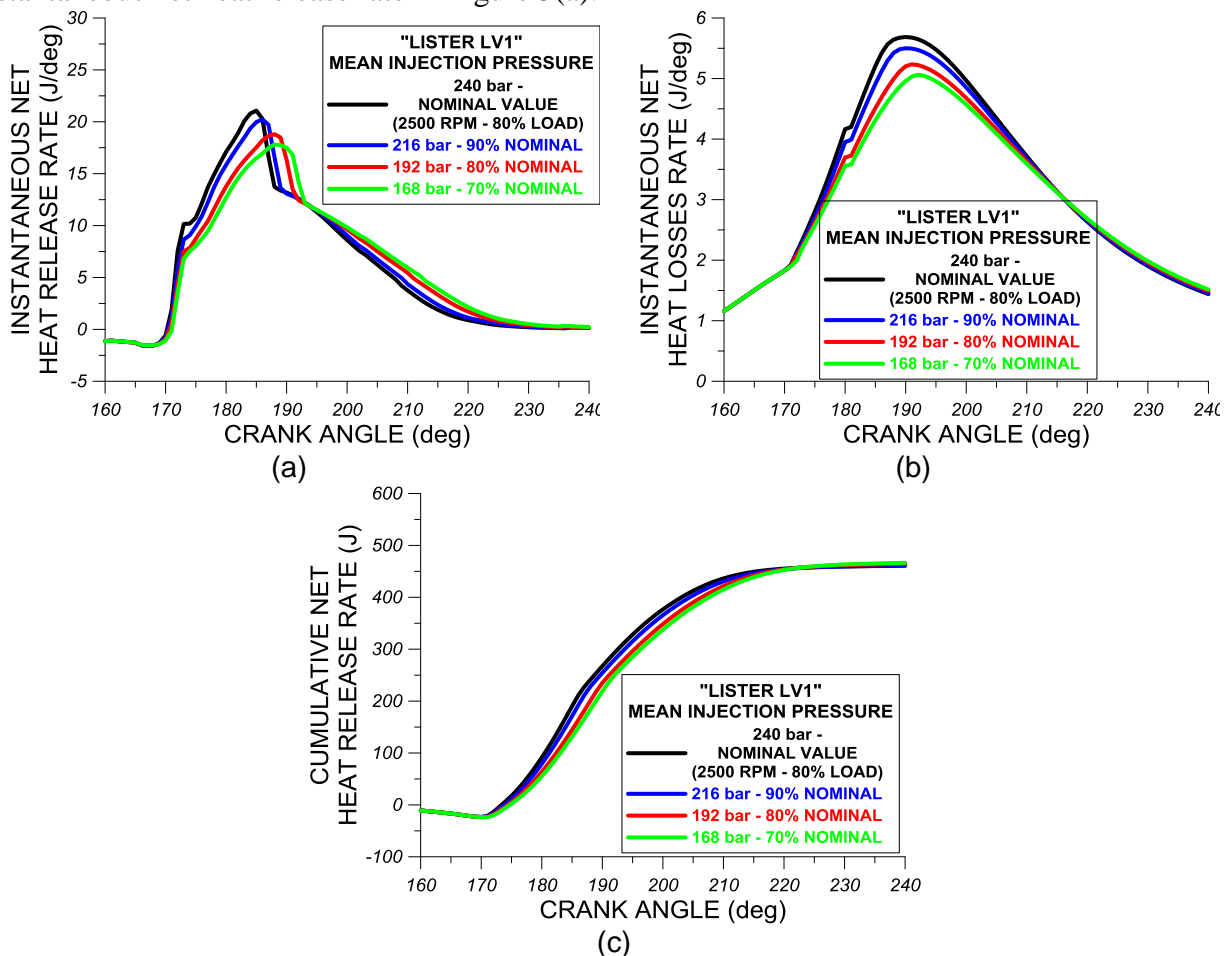

FIGURE 5. Effect of mean injection pressure variation on the predicted (a) instantaneous net heat release rate, (b) instantaneous heat loss rate and (c) cumulative net heat release rate of "Lister LV1" engine. Theoretical results are presented at 240 bars (nominal value of injection pressure), 216 bars (90% of nominal value of injection pressure), 192 bars (80% of nominal value of injection pressure) and 168 bars (70% of nominal value of injection pressure) of fuel injection pressure. The fueling rate of 1.1 kg/h, 240 bars fuel injection pressure and 17.1:1 compression ratio corresponds to "Lister LV1" engine operation at 2500 rpm and at 80% of full load.

Figure 6(a) depicts the effect of varying mean injection pressure on examined engine indicated power. Specifically, results for indicated power are given for four injection pressures namely, 240 bar, 216 bar, 192 bar and 168 bar. As evidenced from Figure 6(a), the reduction of mean injection pressure from 240 to 168 bar results in a very small reduction of indicated power since according to Figure 4(a) the reduction of mean injection pressure does not affect seriously the cylinder pressure during most of the expansion stroke and thus, the reduction of injection pressure has imperceptible influence on main expansion work. The small reduction of indicated power evidenced in Figure 6(a) results, for the same fuel injected mass per engine cycle, in small increase of ISFC. Hence, the reduction of mean injection pressure slightly deteriorates engine power and engine efficiency. According to Figure 6(c) and in relation with the facts observed in Figure 4(a), the reduction of mean injection pressure results in small reduction of peak cylinder pressure primarily due to reduction of cylinder pressure around TDC as a result of the curtailment of the fuel evaporation rate. The small reduction of peak cylinder pressure can be considered as beneficial for the long-term endurance of the examined engine since the reduction of peak cylinder pressure and temperature reduces the thermal and mechanical stress of the cylinder assembly.
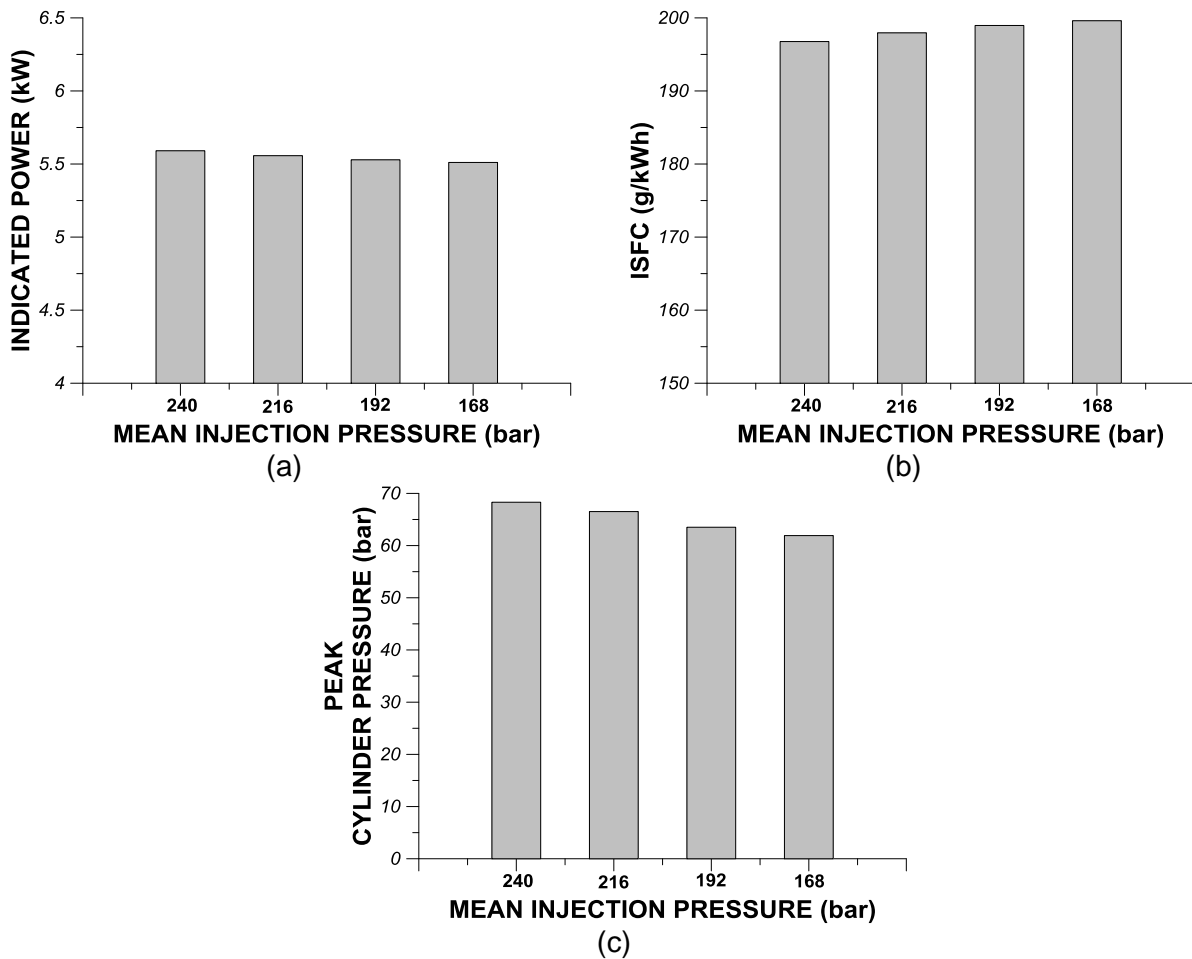
FIGURE 6. Effect of mean injection pressure variation on the predicted (a) indicated power, (b) Indicated Specific Fuel Consumption (ISFC) and (c) peak cylinder pressure of "Lister LV1" engine. Theoretical results are presented at 240 bars (nominal value of injection pressure), 216 bars (90% of nominal value of injection pressure), 192 bars (80% of nominal value of injection pressure) and 168 bars (70% of nominal value of injection pressure) of fuel injection pressure. The fueling rate of 1.1 kg/h, 240 bars fuel injection pressure and 17.1:1 compression ratio corresponds to "Lister LV1" engine operation at 2500 rpm and at 80% of full load.

In Figure 7(a) is shown the variation of ignition angle with mean injection pressure. As evidenced from Figure 7(a), the reduction of mean injection pressure from 240 bar to 168 bar results in a small reduction of ignition angle or in other words, the reduction of mean injection pressure delays the combustion initiation resulting thus, to its shift closer to the TDC. Combustion commencement delay with injection pressure reduction can be ascribed to the delay of combustion pressure rise due to reduction of fuel evaporation rate and subsequently, due to curtailment of premixed combustion rate. Having given that the fuel injection timing remained constant at 15 degrees BTDC for all cases of variable injection pressure, the previously-observed delay of combustion initiation with decreasing injection pressure results, as evidenced from Figure 7(b), in an increase of ignition delay, which reaches up to almost 15% compared to the conventional case of 240 bar mean injection pressure.

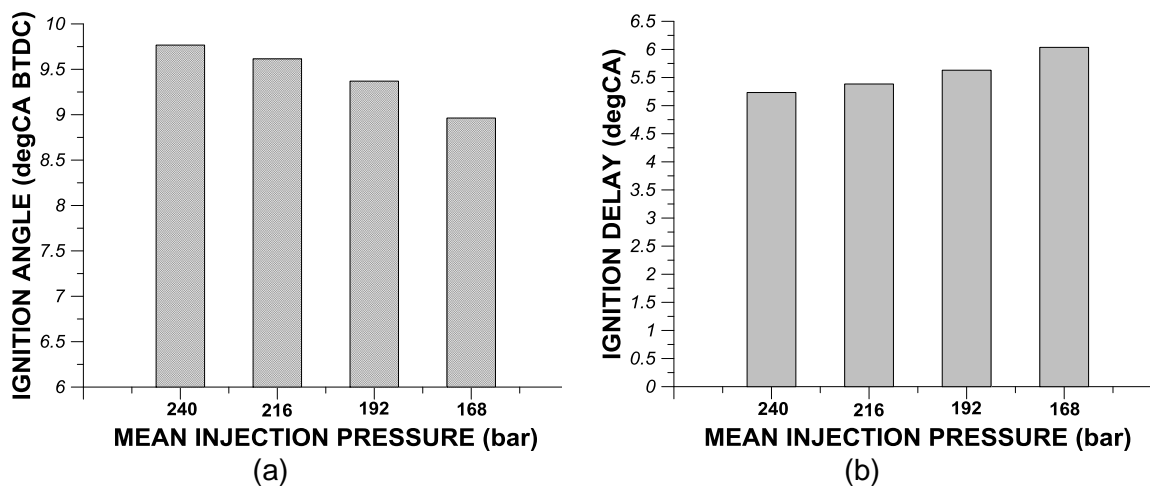(a)   (b)

FIGURE 7. Effect of mean injection pressure variation on the predicted (a) ignition angle and (b) ignition delay. Theoretical results are presented at 240 bars (nominal value of injection pressure), 216 bars (90% of nominal value of injection pressure), 192 bars (80% of nominal value of injection pressure) and 168 bars (70% of nominal value of injection pressure) of fuel injection pressure. The fueling rate of 1.1 kg/h, 240 bars fuel injection pressure and 17.1:1 compression ratio corresponds to "Lister LV1" engine operation at 2500 rpm and at 80% of full load.

In Figures 8(a)-(d) is shown the effect of mean injection pressure variation on the combustion durations of 5% (Figure 8(a)), 25% (Figure 8(b)), 50% (Figure 8(c)) and 90% (Figure 8(d)) of total fuel injected mass per engine cycle. According to all Figures 8(a)-(d) the reduction of mean injection pressure from 240 bar to 168 bar results in an increase of all percentages of fuel combustion duration. In the case of combustion durations of 5% and 25% of total injected fuel (Figures 8(a)-(b)), which correspond to premixed combustion phase, their increase with decreasing mean injection pressure can be attributed to the reduction of premixed combustion intensity. Hence, the reduction of mean injection pressure leads to an increase of the premixed combustion duration of the same fuel injected mass per engine cycle i.e. same fuel quantity takes more time to be burned under premixed conditions. Also according to Figure 8(d), the reduction of mean injection pressure does not only increases premixed combustion durations but also increases – and this is more pronounced in the case of the lowest injection pressure i.e. 168 bar – the combustion duration of 90% fuel injected mass per engine cycle. Hence, the same fuel quantity delays to be burned not only under premixed conditions but also under both premixed and diffusion-controlled conditions and thus, overall it can be stated that the reduction of mean injection pressure affects negatively both premixed and diffusion-controlled combustion phase durations and consequently, deteriorates total combustion duration.
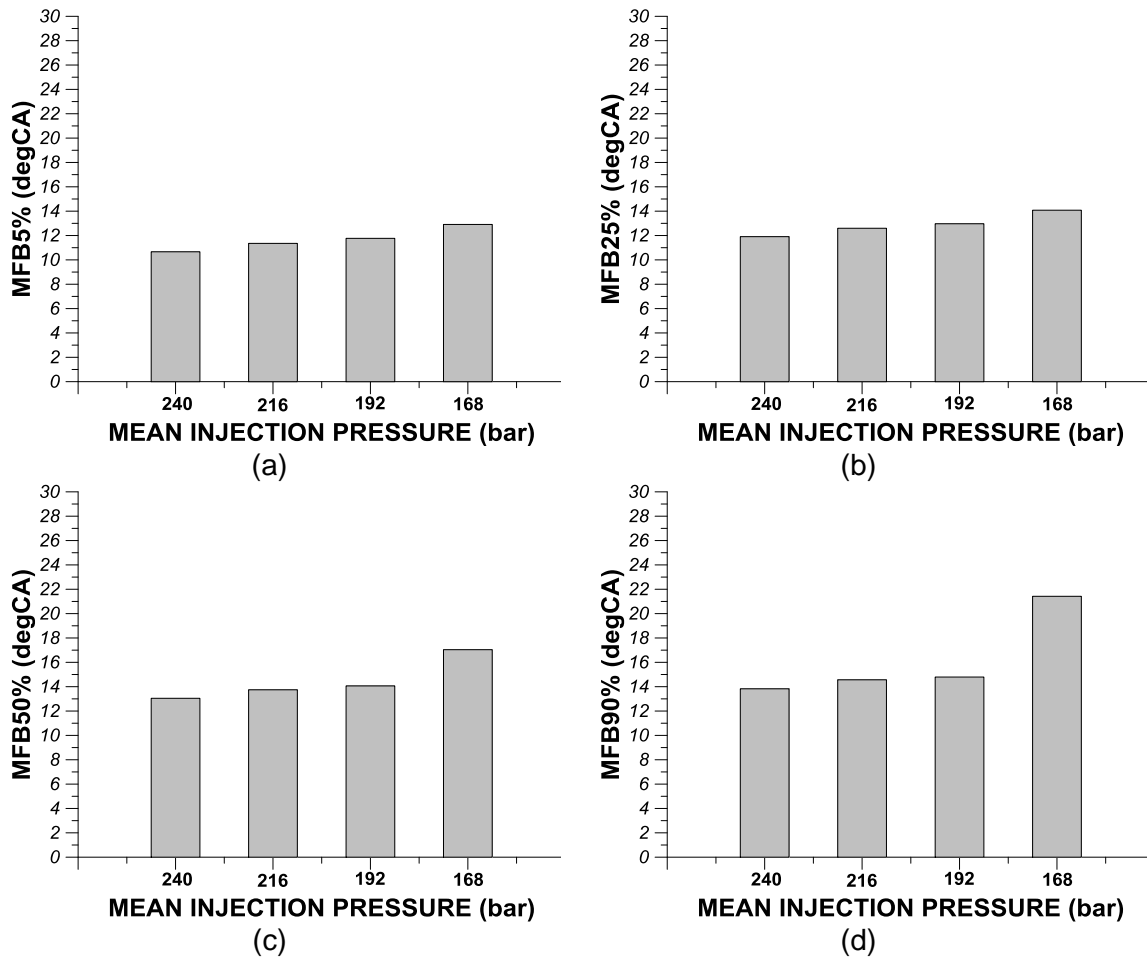
FIGURE 8. Effect of mean injection pressure variation on the predicted combustion duration in crank angle degrees of (a) 5%, (b) 25%, (c) 50% and (d) 90% of fuel injected mass per engine cycle. Theoretical results are presented at 240 bars (nominal value of injection pressure), 216 bars (90% of nominal value of injection pressure), 192 bars (80% of nominal value of injection pressure) and 168 bars (70% of nominal value of injection pressure) of fuel injection pressure. The fueling rate of 1.1 kg/h, 240 bars fuel injection pressure and 17.1:1 compression ratio corresponds to "Lister LV1" engine operation at 2500 rpm and at 80% of full load.

Effect of Fuel Consumption Variation on DI Diesel Engine Performance and Combustion Characteristics

The effect of fuel consumption variation on combustion parameters and performance characteristics of a four-stroke high-speed single-cylinder DI diesel engine ("Lister LV1") is examined in this paragraph. The objective of this investigation is to simulate diesel engine operation in the case the fuel injector does not inject the proper fuel quantity at a specific engine operating condition either due to injector needle lift problem or due to fuel pump improper operation or due to nozzle orifices blocking. Hence, it is considered fuel consumption variation compared to its nominal value, which provides a theoretical cylinder pressure profile using the closed-cycle simulation model that matches the corresponding experimental one at 2500 rpm and

at 80% of full load. It is examined the impact of fuel consumption variation on predicted fuel evaporation rate, cylinder pressure profile, bulk gas temperature profile, indicated power, ISFC, net instantaneous and cumulative heat release rate, ignition angle, ignition delay and combustion durations of 5%, 25%, 50% and 90% of total fuel injected mass per engine cycle. The following fuel consumption values are examined:

- 1.1 kg/h, which corresponds to the nominal value of fuel consumption that provides a theoretical cylinder pressure profile using the multi-zone combustion model that matches the corresponding experimental cylinder pressure profile at 2500 rpm and at 80% load.
- 1.265 kg/h – This value of fuel consumption corresponds to the 115% of the nominal value.
- 0.99 kg/h– This value of fuel consumption corresponds to the 90% of the nominal value.
- 0.88 kg/h - This value of fuel consumption corresponds to the 80% of the nominal value.

For each one of the above-mentioned fuel consumption values are derived theoretical cylinder pressure profiles using the multi-zone combustion model. Initially a simulation was performed at 2500 rpm and at 80% of full load using fuel consumption value equal to 1.1 kg/h, mean injection pressure equal to 240 bar, compression ratio equal to 17.1:1 and injection timing equal to 15 degCA BTDC. At all other cases of fuel consumption, the above-mentioned input values of mean injection pressure, compression ratio and injection timing remained the same to isolate the effect of fuel consumption. Afterwards, the theoretical cylinder pressure profiles derived from the previous computational investigation were supplied to the MATLAB model for performing a heat release rate analysis and for predicting the main combustion parameters and engine performance characteristics at each fuel consumption case.

In Figure 9(a) is shown the effect of fuel consumption variation on predicted fuel evaporation rate using the multi-zone combustion model. Specifically, in Figure 9(a) are given predicted fuel evaporation rates for four fuel consumptions i.e. 1.1 kg/h, 1.265 kg/h, 0.99 kg/h and 0.88 kg/h. As evidenced from Figure 9, the reduction of fuel consumption results in reduction of the effective fuel evaporation period whereas, no significant changes are observed in the peak evaporation rate. In other words, the increase of fuel consumption, as expected, results in a time elongation of the fuel evaporation process shifting thus, combustion to the expansion stroke. Combustion shift to the expansion stroke is verified from Figure 9(b), which shows the effect of fuel consumption variation on the predicted cylinder pressure profile. As evidenced from Figure 9(b), the reduction of fuel consumption results in reduction of cylinder pressure during the entire expansion stroke and thus, in reduction of expansion work. According to Figure 9(c), the reduction of fuel injected mass per engine cycle results in significant reduction of in-cylinder bulk gas temperatures during expansion stroke i.e. after 190 degCA ABDC as a result of the reduction of the fuel evaporation rate. The reduction of bulk gas temperatures inside the combustion chamber during expansion stroke due to reduction of fuel consumption will lead to the significant reduction of exhaust gas temperature at EVO.
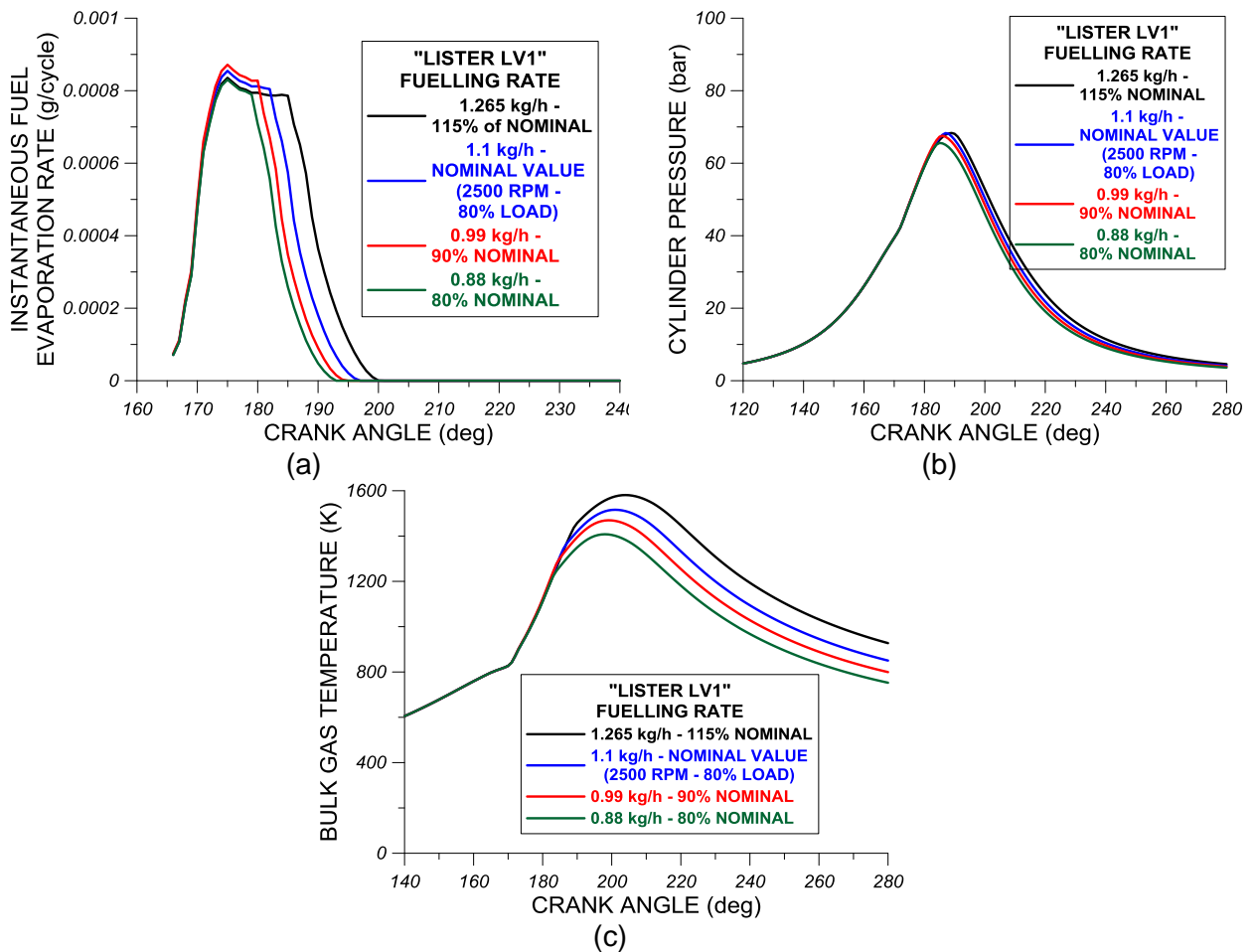
FIGURE 9. Effect of fuel consumption variation on theoretical (a) instantaneous fuel evaporation rate, (b) cylinder pressure and (c) in-cylinder bulk gas temperature profiles of "Lister LV1" engine. Theoretical results are presented at 1.1 kg/h (nominal value of fueling rate), 1.265 kg/h (115% of nominal fueling rate value), 0.99 kg/h (90% of nominal fueling rate value) and 0.88 kg/h (80% of nominal fueling rate value). The fueling rate of 1.1 kg/h, 240 bars fuel injection pressure and 17.1:1 compression ratio corresponds to "Lister LV1" engine operation at 2500 rpm and at 80% of full load.

As evidenced from Figure 10(a), which depicts the effect of fuel consumption variation on instantaneous net heat release rate, the reduction of cylinder pressure and bulk gas temperature during most of the expansion stroke due to the reduction of fuel consumption results in curtailment of combustion intensity during both premixed and diffusion-controlled combustion phases. The highest enhancement of combustion intensity is observed during diffusion-controlled combustion due to the shift of main combustion event to the late expansion stroke. This combustion shift to the late expansion stroke will also result to the considerable increase of in-cylinder generated and exhaust soot emissions. The reduction of fuel consumption and the subsequent reduction of bulk gas temperature results in considerable reduction of instantaneous heat losses rate during expansion stroke as evidenced from Figure 10(b). Finally, the shift of combustion event to the expansion stroke with increasing fuel consumption results in a substantial increase of the cumulative neat heat release rate and thus, to the total net combustion-released thermal energy as expected due to the increase of the supplied fuel heating power.
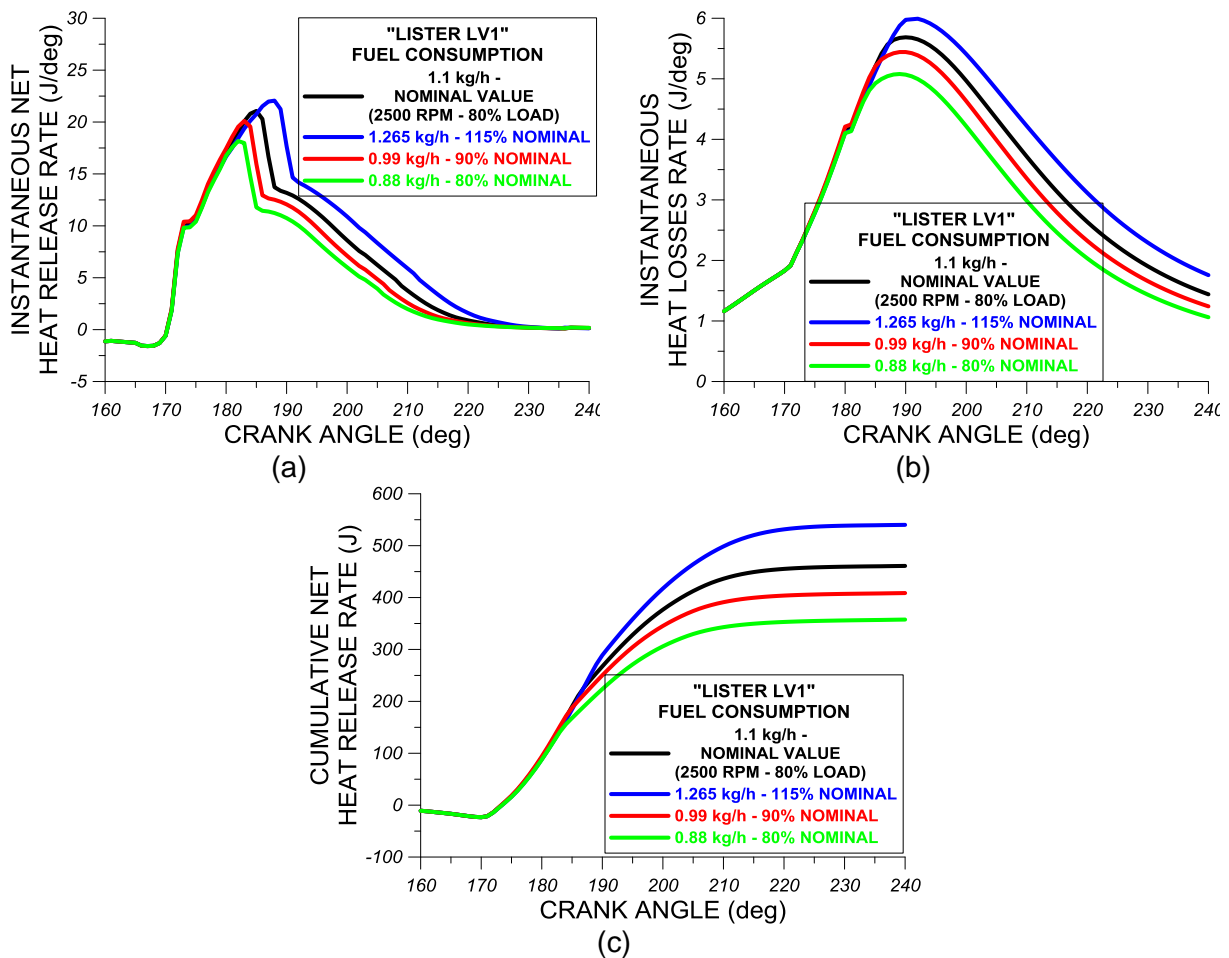
FIGURE 10. Effect of fuel consumption variation on the predicted (a) instantaneous net heat release rate, (b) instantaneous heat loss rate and (c) cumulative net heat release rate of "Lister LV1" engine. Theoretical results are presented at 1.1 kg/h (nominal value of fueling rate), 1.265 kg/h (115% of nominal fueling rate value), 0.99 kg/h (90% of nominal fueling rate value) and 0.88 kg/h (80% of nominal fueling rate value). The fueling rate of 1.1 kg/h, 240 bars fuel injection pressure and 17.1:1 compression ratio corresponds to "Lister LV1" engine operation at 2500 rpm and at 80% of full load.

In Figure 11(a) is shown the effect of varying fuel consumption on the indicated power. As observed from Figure 11(a), the increase of fuel consumption from 1.1 kg/h to 1.265 kg/h results in significant increase of indicated power due to previously-mentioned enhancement of the expansion work. The relative increase of indicated power in this case is 15%. On the other hand, the reduction of fuel consumption from 1.265 kg/h to 0.88 kg/h results in substantial reduction of engine power. The relative reduction of engine indicated power between 1.1 kg/h (i.e. nominal value of fuel consumption) and 0.88 kg/h is 21%. Hence, is proved that the reduction of fuel consumption results in an almost linear reduction of engine power as expected. As evidence from Figure 11(b), the linear reduction of engine power with decreasing fuel consumption results in imperceptible increase of ISFC (i.e. engine efficiency), which reaches up to 1.4% in the case of 0.88 kg/h compared to the nominal case of 1.1 kg/h. According to Figure 11(c), the reduction of fuel consumption results in a small reduction of peak cylinder pressure since the impact of fuel

consumption reduction is less pronounced during premixed combustion phase (i.e. variations in fuel consumption are more evident during diffusion-controlled combustion).
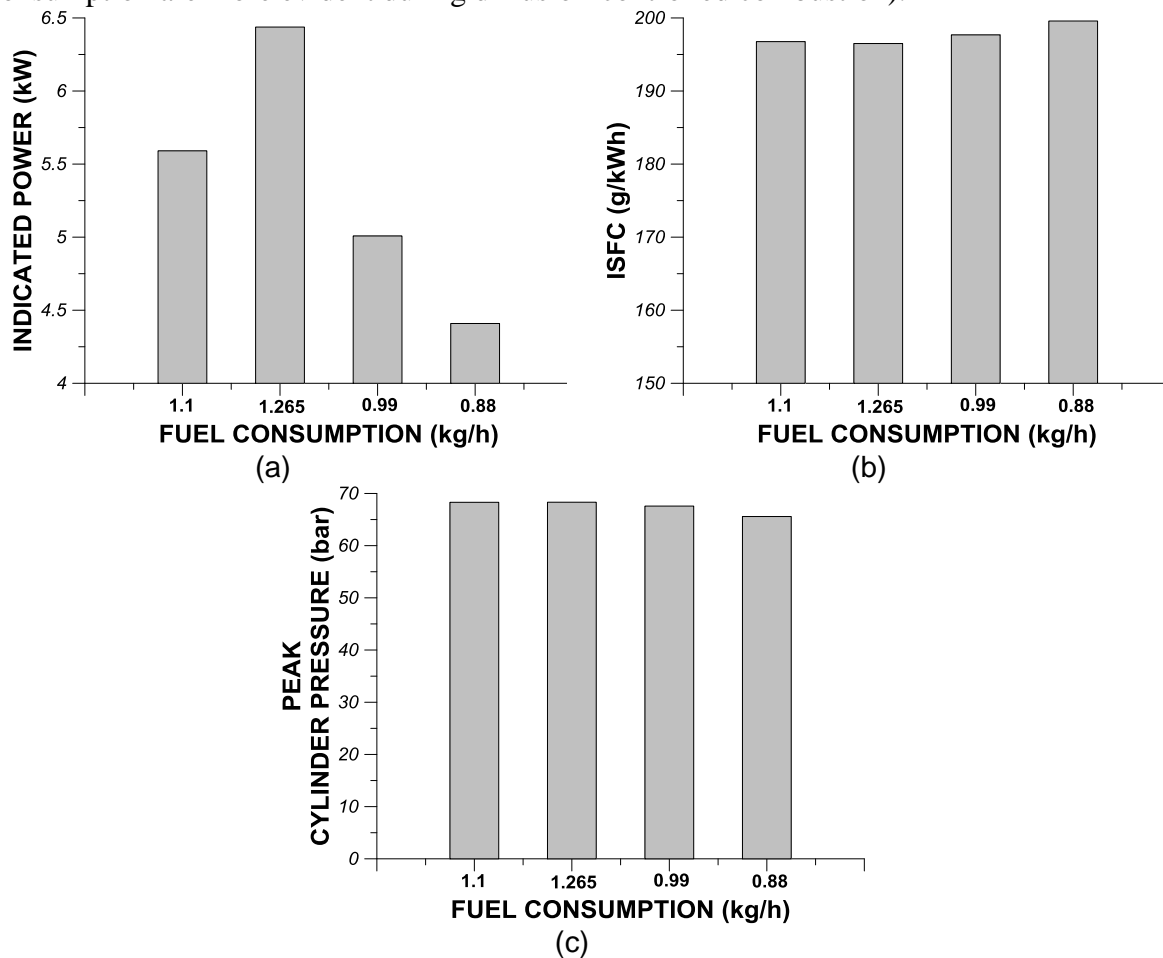

FIGURE 11. Effect of fuel consumption variation on the predicted (a) indicated power, (b) Indicated Specific Fuel Consumption (ISFC) and (c) peak cylinder pressure of "Lister LV1" engine. Theoretical results are presented at 1.1 kg/h (nominal value of fueling rate), 1.265 kg/h (115% of nominal fueling rate value), 0.99 kg/h (90% of nominal fueling rate value) and 0.88 kg/h (80% of nominal fueling rate value). The fueling rate of 1.1 kg/h, 240 bars fuel injection pressure and 17.1:1 compression ratio corresponds to "Lister LV1" engine operation at 2500 rpm and at 80% of full load.

Figure 12(a) shows the effect of fuel consumption variation on ignition angle. As evidenced from Figure 12(a), the reduction of fuel consumption does not bring any noticeable change to the ignition point since the fuel consumption does not affect the physical and chemical preparation pre-combustion mechanism. Consequently, since the injection timing was kept constant at all cases of fuel consumption variation, the invariance of ignition angle with varying fuel consumption results also in imperceptible changes to the ignition delay as evidenced from Figure 12(b).

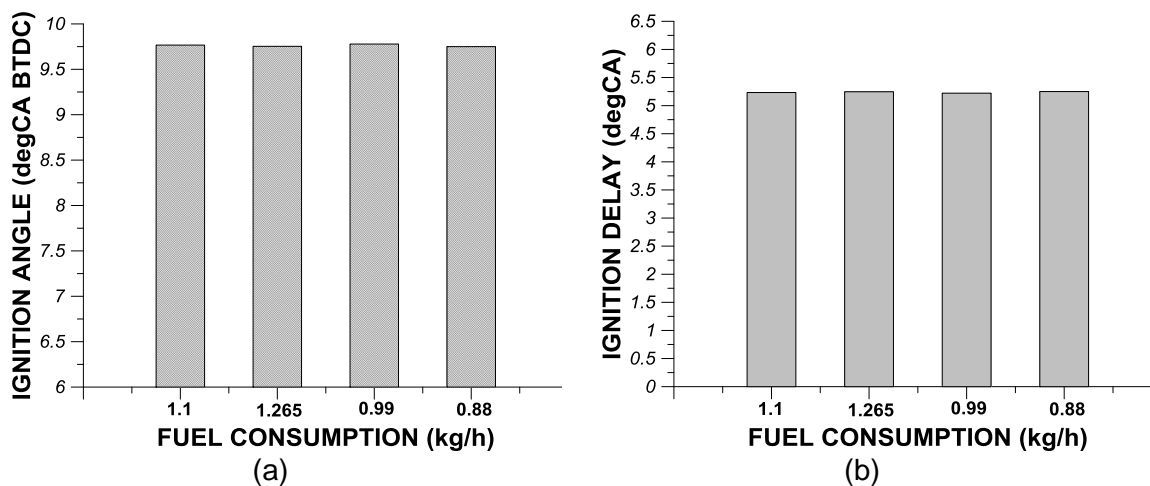(a)   (b)

FIGURE 12. Effect of fuel consumption variation on the predicted (a) ignition angle and (b) ignition delay. Theoretical results are presented at 1.1 kg/h (nominal value of fueling rate), 1.265 kg/h (115% of nominal fueling rate value), 0.99 kg/h (90% of nominal fueling rate value) and 0.88 kg/h (80% of nominal fueling rate value). The fueling rate of 1.1 kg/h, 240 bars fuel injection pressure and 17.1:1 compression ratio corresponds to "Lister LV1" engine operation at 2500 rpm and at 80% of full load.

In Figures 13(a)-(d) is shown the effect of fuel consumption variation on the combustion durations of 5% (Figure 13(a)), 25% (Figure 13(b)), 50% (Figure 13(c)) and 90% (Figure 13(d)) of total fuel injected mass per engine cycle. According to Figures 13(a)-(b) the variation of fuel consumption does not bring serious changes to the combustion durations of 5% and 25% of total fuel injected mass per engine cycle. This can be attributed to the fact that the reduction of fuel consumption primarily affects the second diffusion-controlled stage of combustion and not the initial premixed phase of combustion. Hence, the combustion durations of 5% and 25% of total fuel injected mass do not vary noticeably with fuel consumption variation. The considerable reduction of diffusion-controlled combustion intensity with decreasing fuel consumption results in a slight increase of combustion durations of 50% and 90% of fuel injected mass per engine cycle as evidenced from Figures 13(c)-(d). The curtailment of diffusion-controlled combustion intensity with decreasing fuel consumption especially in the cases of 0.99 kg/h and 0.88 kg/h means that it takes more time for the same fuel quantity to be burned under diffusion-controlled conditions and this results in a slight elongation of the combustion durations of 50% and 90% of total fuel injected mass per engine cycle.
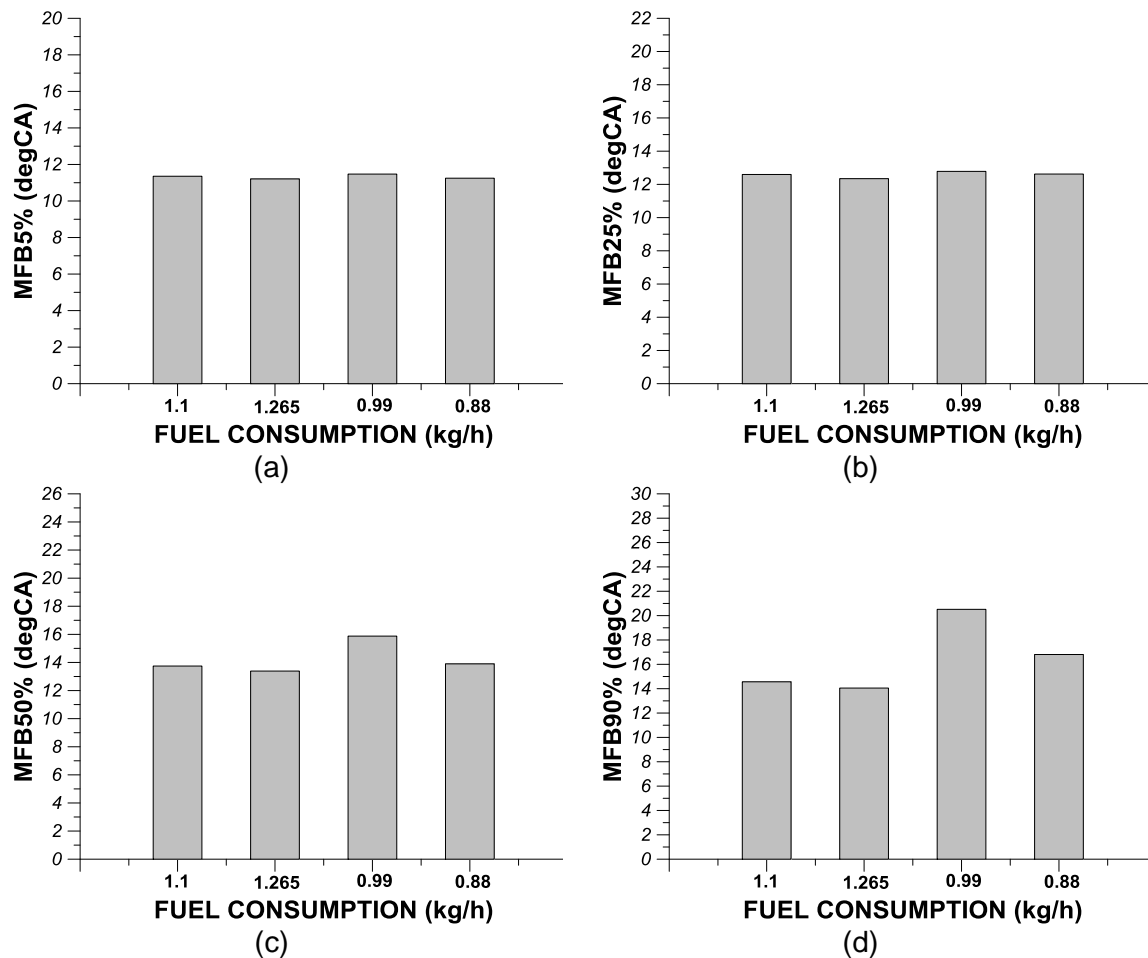
FIGURE 13. Effect of fuel consumption variation on the predicted combustion duration in crank angle degrees of (a) 5%, (b) 25%, (c) 50% and (d) 90% of fuel injected mass per engine cycle. Theoretical results are presented at 1.1 kg/h (nominal value of fueling rate), 1.265 kg/h (115% of nominal fueling rate value), 0.99 kg/h (90% of nominal fueling rate value) and 0.88 kg/h (80% of nominal fueling rate value). The fueling rate of 1.1 kg/h, 240 bars fuel injection pressure and 17.1:1 compression ratio corresponds to "Lister LV1" engine operation at 2500 rpm and at 80% of full load.

Effect of Compression Ratio Variation on DI Diesel Engine Performance and Combustion Characteristics

In this section is examined the impact of compression ratio on engine combustion and performance characteristics of a four-stroke high-speed single-cylinder DI diesel engine ("Lister LV1"). The objective of this investigation is to simulate diesel engine operation in the case of compression loss due to excessive wear of the piston assembly, which is a serious engine fault with direct negative repercussions on engine reliability and availability. Hence, to examine the impact of compression loss on engine combustion mechanism and performance parameters, it was considered four different values of compression ratio i.e. 17.1:1. 16.67:1, 16.25:1 and 15.39:1. The value of 17.1:1 compression ratio in conjunction with 240 bar injection pressure and 1.1 kg/h fuel consumption used as input values to the multi-zone model generate a theoretical cylinder pressure profile that as evidenced in previous section matches the experimental cylinder

pressure profile at 2500 rpm and at 80% load. The other three cases of compression ratio namely 16.67:1, 16.25:1 and 15.39:1 correspond to 97.5%, 95% and 90% of the nominal value of compression ratio (i.e. 17.1:1). Under this investigation, it is examined the impact of compression ratio variation on predicted fuel evaporation rate, cylinder pressure profile, bulk gas temperature profile, indicated power, engine efficiency (i.e. ISFC), instantaneous and cumulative net heat release rate, instantaneous heat losses rate, ignition point and ignition delay and combustion durations of 5%, 25%, 50% and 90% of total fuel injected mass per engine cycle.

Initially a simulation was performed at 2500 rpm and at 80% of full load using fuel consumption value equal to 1.1 kg/h, mean injection pressure equal to 240 bar, compression ratio equal to 17.1:1 and injection timing equal to 15 degCA BTDC. At all other cases of compression ratio, the above-mentioned input values of mean injection pressure, compression ratio and injection timing remained the same to isolate the effect of compression ratio. Afterwards, the theoretical cylinder pressure profiles derived from the previous computational investigation were supplied to the MATLAB model for performing a heat release rate analysis and for predicting the main combustion parameters and engine performance characteristics at each compression ratio case.

In Figure 14(a) is shown the effect of decreasing compression ratio on predicted fuel evaporation rates from the multi-zone combustion model. As observed from Figure 14(a), the reduction of compression ratio does not bring any serious effect on either peak fuel evaporation rates both the duration of fuel evaporation process. On the other hand, the reduction of compression ratio results in reduction of cylinder pressure both during compression stroke and around TDC as evidenced from Figure 14(b). Reduction of cylinder pressure initially during compression stroke and then during the initial stages of combustion can be ascribed to the reduction of peak compression pressure and temperature due to reduction of compression ratio. The variation of cylinder pressure with decreasing compression ratio is reflected on the variation of bulk gas temperature with varying compression ratio. Specifically, according to Figure 14(c), the reduction of compression ratio results in reduction of slight reduction of bulk gas temperature during compression stroke and during the initial stages of combustion.
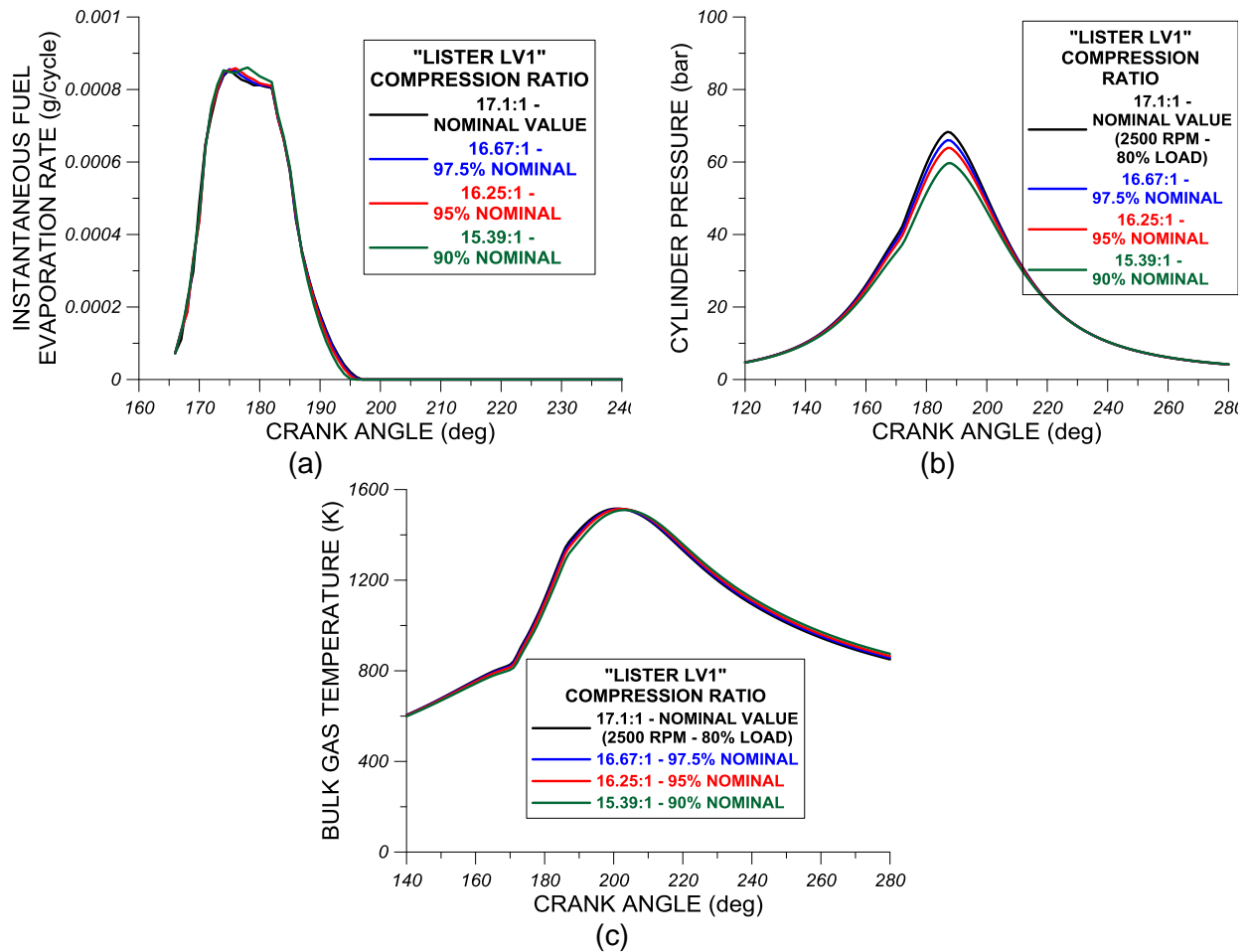
FIGURE 14. Effect of compression ratio variation on theoretical **(a)** instantaneous fuel evaporation rate, **(b)** cylinder pressure and **(c)** in-cylinder bulk gas temperature profiles of "Lister LV1" engine. Theoretical results are presented at 17.1:1 compression ratio (nominal value), 16.67:1 compression ratio (97.5% of nominal value), 16.25:1 compression ratio (95% of nominal value) and 15.39:1 (90% of nominal value). The fueling rate of 1.1 kg/h, 240 bars fuel injection pressure and 17.1:1 compression ratio corresponds to "Lister LV1" engine operation at 2500 rpm and at 80% of full load.

In Figure 15(a) is shown the effect of decreasing compression ratio on the instantaneous net heat release rate. As evidenced from Figure 15(a), the reduction of compression ratio results in a slight reduction of premixed combustion intensity whereas, a slight enhancement of diffusion-controlled combustion intensity is observed with decreasing compression ratio. This means that the reduction of compression ratio results in reduction of total fuel injected mass percentage burned under premixed conditions and in a subsequent slight increase of fuel injected mass portion burned under diffusion-controlled conditions. The reduction of cylinder pressure and most importantly, bulk gas temperature during compression stroke and during the initial stages of combustion results in considerable reduction of instantaneous heat losses rate as observed from Figure 15(b). The reduction of peak compression pressure and temperature due to reduction of compression ratio results in reduction of bulk gas temperature during compression stroke and during the initial stages of combustion affecting thus directly both convection and radiation heat

losses mechanisms. The variations of instantaneous net heat release rate observed with the reduction of compression ratio are reflected to the variation of cumulative net heat release rate. Specifically, as evidenced from Figure 15(c), the reduction of compression ratio results in reduction of cumulative net heat release rate during both stages of diesel combustion mechanism.
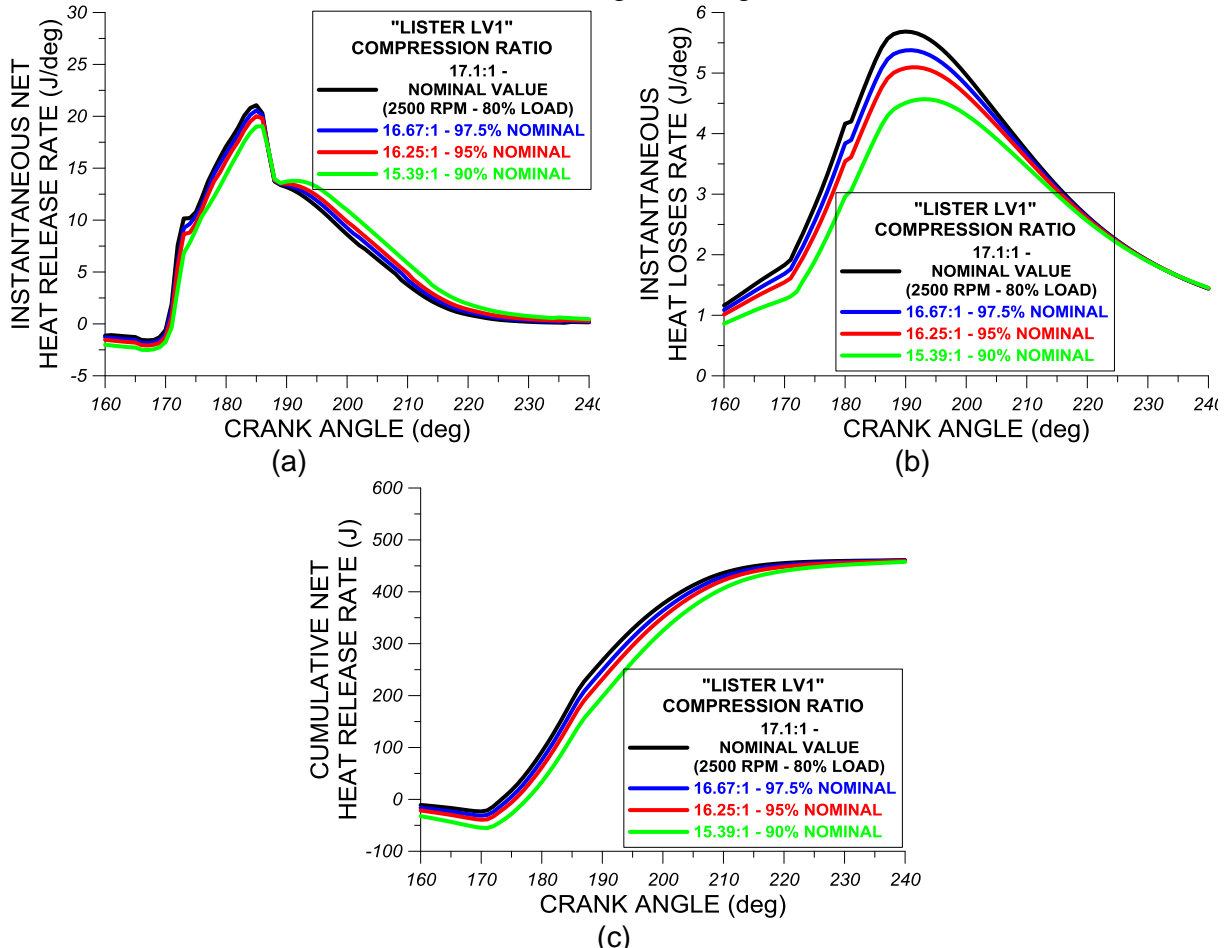

FIGURE 15. Effect of compression ratio variation on the predicted (a) instantaneous net heat release rate, (b) instantaneous heat loss rate and (c) cumulative net heat release rate of "Lister LV1" engine. Theoretical results are presented at 17.1:1 compression ratio (nominal value), 16.67:1 compression ratio (97.5% of nominal value), 16.25:1 compression ratio (95% of nominal value) and 15.39:1 (90% of nominal value). The fueling rate of 1.1 kg/h, 240 bars fuel injection pressure and 17.1:1 compression ratio corresponds to "Lister LV1" engine operation at 2500 rpm and at 80% of full load.

Figure 16(a) shows the effect of compression ratio on engine indicated power. As observed from Figure 16(a), the reduction of compression ratio results in slight decrease of engine indicated power mainly due to the reduction of cylinder pressure during expansion stroke, which potentially overwhelms the slight reduction of compression work during compression stroke. According to figure 16(b), the reduction of compression ratio results in a slight increase of ISFC (i.e. slight deterioration of indicated engine efficiency). The relative deterioration of ISFC between the nominal value of compression ratio (i.e. 17.1:1) and the reduced value of 15.39:1 is 1.5%. The slight reduction of ISFC with decreasing compression ratio is attributed to the slight reduction of indicated power for the same fuel consumption as previously observed. Finally, in

Figure 16(c) is shown the effect of compression ratio on peak cylinder pressure. As evidenced from Figure 16(c), the reduction of compression ratio results in reduction of peak cylinder pressure due to reduction of cylinder pressure profile around TDC as witnessed in Figure 14(b). The relative reduction of peak cylinder pressure caused by the reduction of compression ratio from 17.1:1 to 15.39:1 is 12.6%.
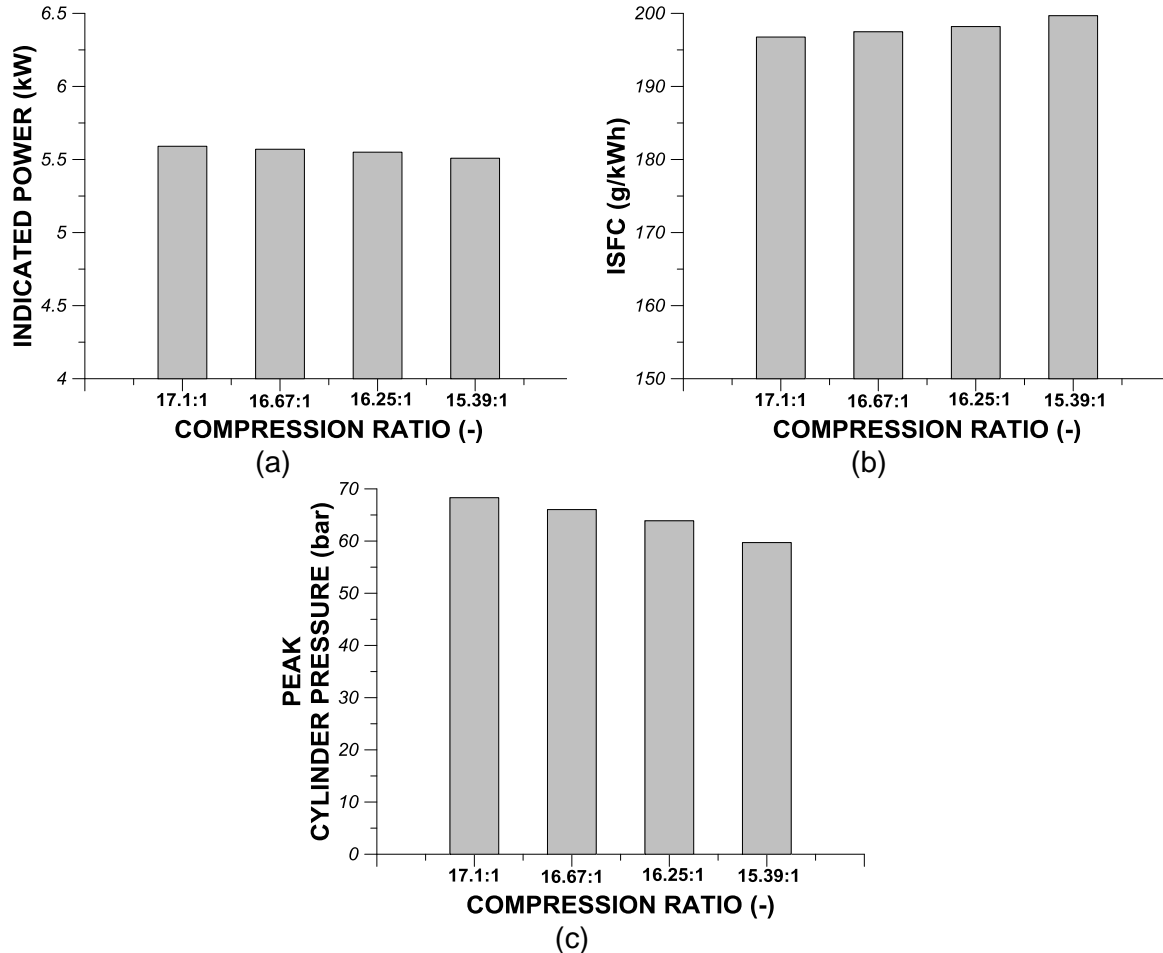

FIGURE 16. Effect of compression ratio variation on the predicted (a) indicated power, (b) Indicated Specific Fuel Consumption (ISFC) and (c) peak cylinder pressure of "Lister LV1" engine. Theoretical results are presented at 17.1:1 compression ratio (nominal value), 16.67:1 compression ratio (97.5% of nominal value), 16.25:1 compression ratio (95% of nominal value) and 15.39:1 (90% of nominal value). The fueling rate of 1.1 kg/h, 240 bars fuel injection pressure and 17.1:1 compression ratio corresponds to "Lister LV1" engine operation at 2500 rpm and at 80% of full load.

Figures 17(a) and 17(b) depict the impact of decreasing compression ratio on ignition angle and ignition delay respectively. As observed from Figure 17(a), the reduction of compression ratio results in reduction of ignition angle or in other words, the reduction of compression of compression ratio shifts combustion initiation closer to TDC. The delay of combustion commencement with decreasing compression ratio can be attributed to the reduction of cylinder pressure and temperature during fuel injection process. This means that fuel physical and chemical preparation processes are less promoted due to lower in-cylinder pressures and temperatures leading thus, to delayed combustion initiation. The delay of combustion

commencement (i.e. reduction of ignition angle) in conjunction with the constant injection timing (i.e. 15 degCA BTDC) at all cases of compression ratio results in an increase of ignition delay as evidenced from Figure 17(b). The relative deterioration of ignition delay with decreasing compression ratio reaches up to 16.4% when comparing the cases of nominal compression ratio (i.e. 17.1:1) and the reduced compression ratio of 15.39:1.
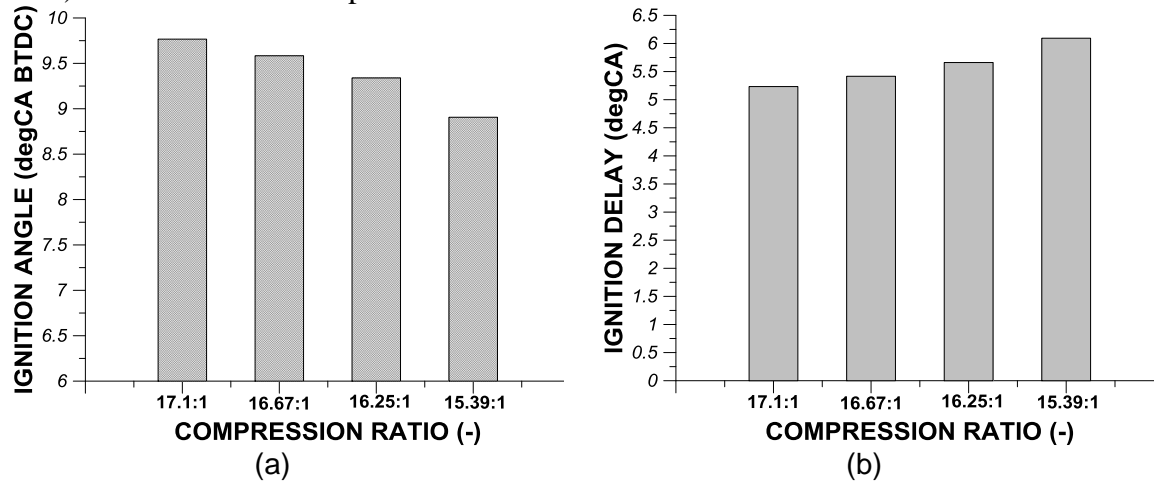

FIGURE 17. Effect of compression ratio variation on the predicted (a) ignition angle and (b) ignition delay. Theoretical results are presented at 17.1:1 compression ratio (nominal value), 16.67:1 compression ratio (97.5% of nominal value), 16.25:1 compression ratio (95% of nominal value) and 15.39:1 (90% of nominal value). The fueling rate of 1.1 kg/h, 240 bars fuel injection pressure and 17.1:1 compression ratio corresponds to "Lister LV1" engine operation at 2500 rpm and at 80% of full load.

Figures 18(a)-(d) illustrate the effect of compression ratio variation on the combustion durations of 5% (Figure 18(a)), 25% (Figure 18(b)), 50% (Figure 18(c)) and 90% (Figure 18(d)) of total fuel injected mass per engine cycle. According to Figures 18(a)-(b) the reduction of compression ratio results in the increase of combustion durations of 5% and 25% of total fuel injected mass per engine cycle. This means that the reduction of compression ratio, which affected negatively the intensity of premixed combustion, results in the elongation of the crank angle duration required for the same fuel injected quantity to be burned under premixed conditions. As evidenced also from Figures 18(c) and mainly from Figure 18(d), the reduction of compression ratio results in the increase of the combustion durations of 50% and 90% of total fuel injected mass per engine cycle. Hence, not only the premixed combustion phase is prolonged but also the highest portion of combustion duration (i.e. 90%) is prolonged with decreasing compression ratio underlying that both diesel combustion phases (i.e. premixed and diffusion-controlled) are prolonged with decreasing compression ratio. In other words, it takes more time in crank angle degrees for the same fuel injected mass to be burned under both premixed and diffusion-controlled conditions.
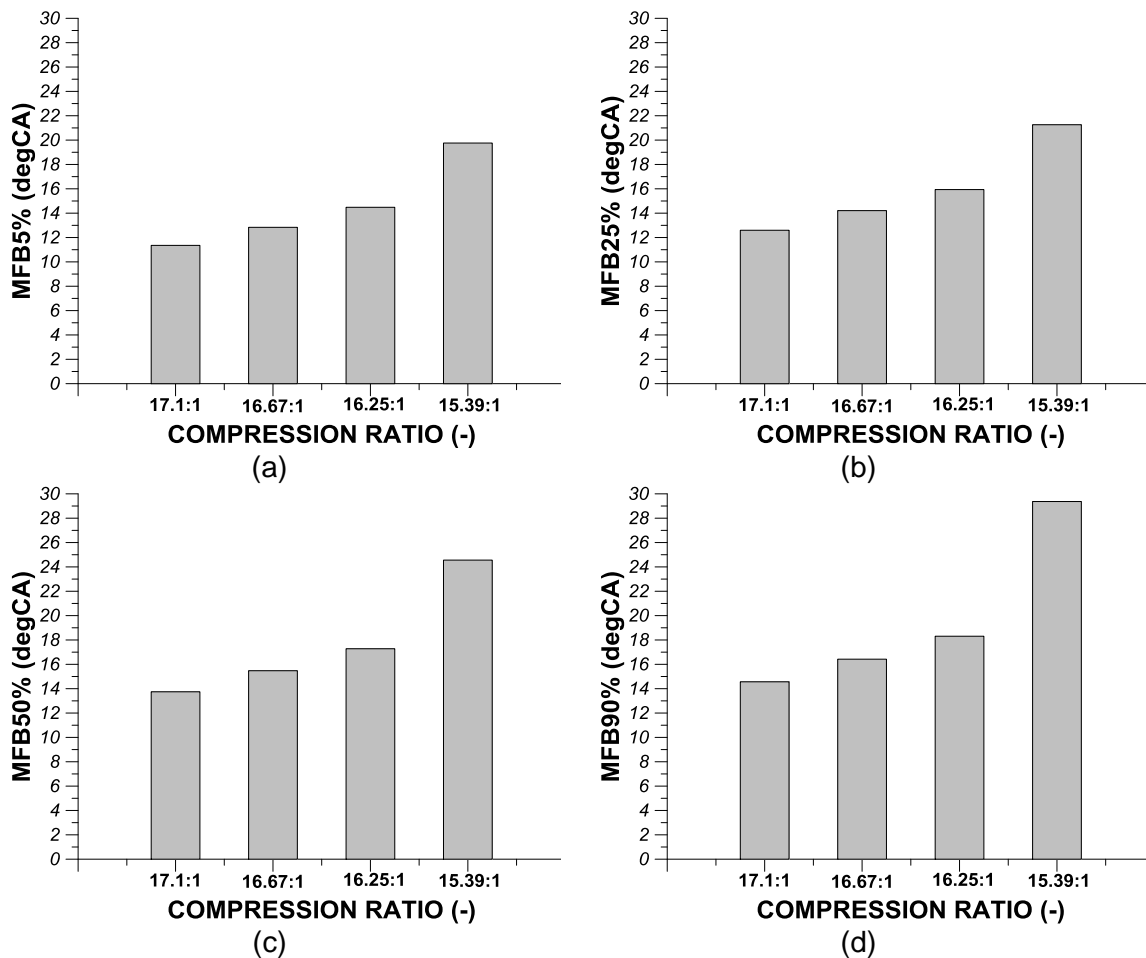
FIGURE 18. Effect of compression ratio variation on the predicted combustion duration in crank angle degrees of (a) 5%, (b) 25%, (c) 50% and (d) 90% of fuel injected mass per engine cycle. Theoretical results are presented at 17.1:1 compression ratio (nominal value), 16.67:1 compression ratio (97.5% of nominal value), 16.25:1 compression ratio (95% of nominal value) and 15.39:1 (90% of nominal value). The fueling rate of 1.1 kg/h, 240 bars fuel injection pressure and 17.1:1 compression ratio corresponds to "Lister LV1" engine operation at 2500 rpm and at 80% of full load.

CONCLUSIONS

In the present study a multi-zone combustion model was used to simulate the close-cycled operation of naturally aspirated single-cylinder DI diesel engine ("Lister LV1") under various values of mean injection pressure, fuel consumption and compression ratio. The main objective of this investigation was to simulate diesel engine operation in the case of faulty operation of the fuel injection system simulated by reduced mean injection pressure and reduced fuel injected mass per engine cycle compared to the corresponding nominal values at a certain engine operating point (i.e. 2500 rpm and 80% load). Also, another objective of this examination was to simulate diesel engine operation in the case of degraded compression quality, which was modelled as compression ratio reduction compared to the corresponding nominal value at 2500 rpm and at 80% load. The multi-zone combustion model after experimental verification was used to derive theoretical results for fuel evaporation rate, cylinder pressure and bulk gas temperature

for each examined case of mean injection pressure, fuel consumption and compression ratio. Afterwards, the predicted cylinder pressure profiles were supplied to a computational model developed in MATLAB under a diploma thesis for performing a heat release rate analysis and for deriving corresponding engine combustion characteristics and performance parameters for all cases of diesel engine faulty operation examined. The assessment of the theoretical results for combustion parameters and performance characteristics at all diesel engine faulty operation cases examined lead to the derivation of the following conclusions:

The reduction of mean injection pressure resulted in:
- Reduction of fuel evaporation rate and elongation of fuel evaporation process.
- Decrease of cylinder pressure around TDC and subsequent reduction of peak cylinder pressure.
- Reduction of bulk gas temperature around TDC.
- Curtailment of premixed combustion intensity and enhancement of diffusion-controlled combustion intensity.
- Reduction of instantaneous heat losses rate due to reduction of bulk gas temperature.
- Slight reduction of engine indicated power and small deterioration of indicated engine efficiency (i.e. ISFC).
- Increase of ignition delay due to shift of combustion initiation closer to TDC.
- Increase of durations of both premixed and diffusion-controlled combustion phases.

The reduction of fuel consumption resulted in:
- Reduction of fuel evaporation process duration.
- Curtailment of cylinder pressure during expansion stroke with direct negative effects on the expansion work and subsequent small decrease of peak cylinder pressure.
- Reduction of bulk gas temperature during expansion stroke.
- Significant reduction of diffusion combustion intensity.
- Reduction of heat losses during expansion stroke.
- Significant reduction of indicated power and small increase of ISFC.
- No serious effect on ignition angle and ignition delay.
- Small increase of 90% combustion duration due to reduction of diffusion-controlled combustion intensity.

The reduction of fuel consumption resulted in:
- Reduction of fuel evaporation process duration.
- Curtailment of cylinder pressure during expansion stroke with direct negative effects on the expansion work and subsequent small decrease of peak cylinder pressure.
- Reduction of bulk gas temperature during expansion stroke.
- Significant reduction of diffusion combustion intensity.
- Reduction of heat losses during expansion stroke.
- Significant reduction of indicated power and small increase of ISFC.
- No serious effect on ignition angle and ignition delay.
- Small increase of 90% combustion duration due to reduction of diffusion-controlled combustion intensity.

The reduction of compression ratio resulted in:
- No serious effect on fuel evaporation rate.
- Reduction of cylinder pressure during late compression stroke and around TDC, which resulted in small decrease of peak cylinder pressure.

- Small reduction of bulk gas temperature around TDC.
- Small decrease of premixed combustion intensity and small enhancement of diffusion-controlled combustion intensity.
- Reduction of heat losses rate during compression stroke and around TDC.
- Small reduction of engine indicated power and small deterioration of engine ISFC.
- Reduction of ignition angle with respect to TDC and increase of ignition delay.
- Increase of both premixed and total combustion durations.

Overall, it can be stated that the reduction of mean injection pressure and compression ratio affects directly the combustion mechanism since they resulted in an increase of ignition delay and thus, to a shift of combustion to the expansion stroke with direct negative effects of exhaust gas temperature at EVO and on particulate emissions formed during diffusion-controlled combustion. The reduction of mean injection pressure and compression ratio also affected negatively both the duration of premixed combustion phase and the total combustion duration. On the other hand, the reduction of fuel consumption due to reduction of the engine supplied heating power has a direct negative effect on engine power and engine efficiency whereas, did not affect seriously the main combustion characteristics such as ignition angle, ignition delay and combustion duration. All faulty engine operation cases examined in the present study (i.e. faulty operation of fuel injection system either expressed as reduction of injection pressure or reduction of fuel injected mass per engine cycle and faulty operation of the piston-ring assembly expressed as loss of compression) have a direct negative impact on engine operability, availability and reliability and for this reason, each faulty case requires the undertake of specific maintenance actions such as the replacement of excessive wear rings in case of compression loss for the restoration of engine availability and reliability.

ACKNOWLEDGEMENTS

NOMENCLATURE

A	area, m^2
c	constant
c_v	specific heat capacity under constant volume, J/(kgK)
D_b	piston bowl diameter, m
D_{ho}	injector nozzle orifice diameter, m
D_{inj}	injector hole diameter, m
D_{SM}	Sauter mean diameter, m
E	activation energy, J/kmol
F	zone area, m^2
FA_{st}	fuel-air stoichiometric ratio (by mass)
F_{ho}	nozzle hole discharge area, m^2
h	convective heat transfer coefficient, $W/(m^2K)$

I	moment of inertia of trapped mass, kgm^2
k_{if}	forward reaction rate constant for the "ith" reaction
l	length, m
m	mass, kg
M	torque, Nm
n	axial velocity exponent
nr	radial zone number
P	pressure, Pa
$\dot{Q}$	heat exchange rate, W
r	radial distance, m
R	radius, m
r_0	radius of nozzle hole, m
R_i	one-way reaction rate for the "ith" reaction
R_{mol}	universal gas constant, J/(kmolK)
R_p	piston radius, m
S_{pr}	ignition delay integral
T	temperature, K
t	time, s
u	zone velocity, m/s
$\bar{u}$	mean velocity, m/s
u_{inj}	injection velocity, m/s
u_p	instantaneous piston velocity, m/s
u_r	radial zone velocity, m/s
u_t	targential air velocity, m/s
u_T	turbulent velocity, m/s
u_{tr}	radial component of targential zone velocity, m/s
u_{tx}	axial component of targential zone velocity, m/s
u_x	axial zone velocity, m/s
V	volume, m^3
W	air angular velocity, rad/s
w	wall jet velocity, m/s
X	jet penetration, m

Greek

α	initial jet angle, rad
δ	wall jet thickness, m
ΔP	pressure difference, Pa
Δφ	calculation step
θ	angle of zone with respect to jet axis, rad
λ	thermal conductivity, W/(mK)
μ	dynamic viscosity, kg/(ms)
ν	kinematic viscosity, m^2/s
ρ	density, kg/m^3
σ	Stefan-Boltzmann constant, $W/(m^2K^4)$

Subscripts

a	air
b,bu	burnt

car   characteristic
ev   evaporated
f   fuel
g   gas
ho   hole
i   zone (i)
inj   injection
pr   preparation
s   soot
SM   Sauter mean
st   stoichiometric
t   targential
T   turbulent
w   wall
x,y   coordinates
0   initial step conditions
1   final step conditions

Abbrevations
ABDC after bottom dead centre
ATDC after top dead centre
BTDC before top dead center
CA   crank angle
RMS   root mean square
SMD   Sauter mean diameter

Dimensionless Numbers
Pr   Prandtl number
Re   Reynolds number
We   Weber number

REFERENCES

1. J.B. Heywood, Internal Combustion Engine Fundamentals, New York: McGraw-Hill, 1988.
2. D.T. Hountalas, Prediction of marine diesel engine performance under fault conditions, Applied Thermal Engineering, 20, 1753 – 1783 (2000).
3. V.T. Lamaris and D.T. Hountalas, A general-purpose diagnostic technique for marine diesel engines – Application on the main propulsion and auxiliary diesel units of a marine vessel, Energy Conversion and Management, 51, 740 – 753 (2010).
4. N.B. Jones and Yu-Hua Li, A review of condition monitoring and fault diagnosis for diesel engines, Tribotest, 6-3, (2000).
5. R. Jiang and X. Yan, "Condition Monitoring of Diesel Engines", In: Complex System Maintenance Handbook. Springer Series in Reliability Engineering. Springer, London, (2008).
6. G.J.J. Oskam, Optimizing Diesel Engine Condition Monitoring, MSc Thesis, Faculty of Mechanical, Maritime and Materials Engineering, Delft University of Technology, (2014).
7. D.T. Hountalas and A.D. Kouremenos, Development and application of a fully automatic troubleshooting method for large marine diesel engines, Applied Thermal Engineering 19, 299-324, (1999)

8. L. Xingyu, S. Gequn, D. Lihui, W. Bin and Y. Kang, "Progress and Recent Trends in the Torsional Vibration of Internal Combustion Engines", Advances in Vibration Analysis Research, IntechOpen, (2011), DOI: 10.5772/16222.

9. S.H. Gawande, L.G. Navale, M.R. Nandgaonkar, D.S. Butala and S. Kunamalla, Fault Detection of Inline Reciprocating Diesel Engine: A Mass and Gas-Torque Approach, Advances in Acoustics and Vibration, Hindawi Publishing Corporation, 2012, Article ID 314706, (2012), doi:10.1155/2012/314706

10. Y. Alhouli, A. Alkhadeli, A. Alzayedi, M. Alardhi and A.I. Abed, Study of Diesel Engine Vibration Condition Monitoring", Global Journal of Researches in Engineering: J General Engineering, 15(6), (2015).

11. J. Orn J., Vibration Guideline for Large Diesel Engines, BSc Thesis, Mechanical and Production Engineering, Vaasa, (2014).

12. H. Raposo, J-T. Farinha, I. Fonseca and L. Andrade Ferreira, Condition Monitoring with Prediction Based on Diesel Engine Oil Analysis: A Case Study for Urban Buses, Actuators, MDPI, 8,14, (2019), doi:10.3390/act8010014.

13. Z. Li, X. Yan, Z. Guo, Y. Zhang, C. Yuan and Z. Peng, Condition Monitoring and Fault Diagnosis for Marine Diesel Engines using Information Fusion Techniques, Electronics and Electrical Engineering. – Kaunas: Technologija, 7(123), 109–112, (2012).

14. T.C. Zannis, Thermodynamic Analysis and Experimental Investigation of the Effect of Liquid Fuels on Diesel Engines, PhD Thesis, School of Mechanical Engineering, National Technical University of Athens, (2006).

15. R.G. Papagiannakis, Study of the Behaviour of Diesel Engines with the Use of Liquid and Gaseous Fuels, PhD Thesis, School of Mechanical Engineering, National Technical University of Athens, Greece, (2002).

16. D.A. Kouremenos, C.D. Rakopoulos and D.T. Hountalas, Multi-zone Combustion Modelling for the Prediction of Pollutants Emissions and Performance of DI Diesel Engines, SAE Transactions, J. of Engines, 106, 940-957, (1997). SAE Paper No. 970635.

17. C.D. Rakopoulos and D.T. Hountalas, Development and Validation of a 3-D Multi-zone Combustion Model for the Prediction of a DI Diesel Engine Performance and Pollutant Emissions, SAE Transactions, J. of Engines, 107, 1413–1429, (1998). SAE Paper No. 981021.

18. C.D. Rakopoulos, D.T. Hountalas, G.N. Taklis and E.I. Tzanos, Analysis of Combustion and Pollutants Formation in a Direct Injection Diesel Engine using a Multi-zone Model, Int. J. Energy Research, 19, 63-88, (1995).

19. C.D. Rakopoulos, D.T. Hountalas and T.C. Zannis, Theoretical Study Concerning the Effect of Oxygenated Fuels on DI Diesel Engine Performance and Emissions, SAE Spring Fuels & Lubricants Meeting & Exhibition, Society of Automotive Engineers (SAE), June 8-10, (2004), Toulouse, France, SAE Paper No 2004-01-1838.

20. T.C. Zannis, E.I. Pariotis, D.T. Hountalas and C.D. Rakopoulos, Effects of Air-Side and Fuel-Side Oxygen Addition on DI Diesel Engine Performance and Pollutant Emissions, Energy Conversion and Management 48(11), 2962-2970, (2007).

21. W.J.D. Annand, Heat Transfer in the Cylinders of Reciprocating Internal Combustion Engines, Proc. Instn Mech. Engrs, 177, 973-990, 1963.

22. D.A. Kouremenos, C.D. Rakopoulos and D.T. Hountalas, Thermodynamic Analysis of Indirect Injection Diesel Engines by Two-zone Modelling of Combustion, Trans. ASME, J. Engineering for Gas Turbines and Power, 112, 138-159, (1990).

23. D.A. Kouremenos, C.D. Rakopoulos and D.T. Hountalas, Thermodynamic Analysis of Divided Combustion Chamber Diesel Engine, VDI Forschung Ing.-Wesens, 54, 73-81, (1988).

24. Kamel M. and Watson N., Heat Transfer in the Indirect Injection Diesel Engine, SAE Paper No. 790826, (1979).

25. B.E. Launder and D.B. Spalding, Mathematical Models of Turbulence, Academic Press, London, (1972).

26. D.A. Willis, W.E. Meyer and C. Birnie, Mapping of Airflow Patterns in Engines with Induction Swirl, SAE Paper No. 660093, (1966).
27. J.C. Dent and J.A. Derham, Air Motion in a Four-Stroke Direct Injection Diesel Engine, Proc. Inst. Mech. Engrs, 188, 269-280, (1974).
28. J.I. Ramos, Internal Combustion Engine Modelling, New York: Hemisphere, (1989).
29. M.B. Glauert, The wall jet, J. Fluid Mechanics, 1, 625-643, (1956).
30. A. Idoum, J.P. Packer, F.J. Wallace and S.J. Charlton, An Experimental and Analytical Study of Jet Impingement and Wall Jets in High Swirl DI Diesel Engine using the Hydraulic Analogy, SAE Paper No. 850263, (1985).
31. H. Hiroyasu, T. Kadota and M. Arai, Development and Use of a Spray Combustion Modelling to Predict Diesel Engine Efficiency and Pollutant Emissions, Bulletin JSME, 26(214), 569-576, (1983).
32. G.L. Borman and J.H. Johnson, Unsteady Vaporization Histories and Trajectories of Fuel Drops injected into Swirling Air, SAE Paper 598C, National Powerplant Meeting, Philadelphia, PA, (1962).
33. D.A. Kouremenos, C.D. Rakopoulos and E.A. Yfantis, A Fortran Program for Calculating the Evaporation Rates in Diesel Engine Fuel Sprays, Advances in Engineering Software, 15, 67-71, (1992).
34. D.A. Assanis, Z.S. Filipi, S.B. Fiveland and M. Syrimis, A Predictive Ignition Delay Correlation under Steady-State and Transient Operation of a Direct Injection Diesel Engine, Trans. ASME, J. of Engineering for Gas Turbines and Power, 125(2), 450-457, (2003).
35. D. Hodgetts and H.D. Shroff, More on the Formation of Nitric Oxide in a Diesel Engine, Conference on "Combustion in Engines", Inst. Mech. Engrs, paper C95/75, 129-138, (1975).
36. C.R. Ferguson, Internal Combustion Engines, New York: John Wiley, (1986).
37. C.D. Rakopoulos, D.T. Hountalas, E.I. Tzanos and G.N. Taklis, A Fast Algorithm for Calculating the Composition of Diesel Combustion Products using 11 Species Chemical Equilibrium Scheme, Advances in Engineering Software, 19, 109-119, (1994).
38. R.J.B. Way, Methods of Determination and Composition and Thermodynamic Properties of Combustion Products for Internal Combustion Engines Calculations, Instn. Mech. Engrs, 190, 687-697, (1977).
39. C. Olikara and G.L. Borman, A Computer Program for Calculating Properties of Equilibrium Combustion Products with Some Applications to I.C. Engines, SAE Paper No.750468, (1975).
40. C.W. Vickland, F.M. Strange, R.A. Bell and E.S. Starkman, A Consideration of the High Temperature Thermodynamics of Internal Combustion Engines, SAE Transactions, 70, 785-793, (1962).